Theory of Condensed Matter and New Materials

Leaders: V.A. Osipov and J. Brankov

Projects:

Physical properties of complex materials and nanostructures

Spokespersons: N.M. Plakida, V.A. Osipov, G. Roepke

Mathematical Problems of Many-Particle Systems

Spokesperson: V.B. Priezzhev, V.I. Yukalov

Main topics

- Strongly correlated systems (high-Tc superconductors, complex magnetic systems)
- Physics of Nanostructures (carbon nanosystems, layered structures, BEC in traps, fractal systems)
- Modern problems of statistical mechanics (sandpile model, random walk models, etc)

Топология и геометрия в современной теории конденсированных сред на примере графена и тд

- Условная классификация:

- Топологические кристаллы
- Топологические дефекты
- Топологические возбуждения

Топологические кристаллы

Topology in Condensed Matter Physics

seminar: May 13 - July 31, 2002

Scientific Coordinators:

Maurice Kleman (Universitй Paris, VI, France)
Michael Monastyrsky (ITEP Moscow, Russia)
Sergei Novikov (University of Maryland, USA and Landau Institute for Theoretical Physics, Russia)
Organisation:

(MPIPKS Dresden, Germany)

Картинки

Topological Defects in Carbon Nanocrystals

Vladimir A. Osipov

Bogoliubov Laboratory of Theoretical Physics, Joint Institute for Nuclear Research, 141980 Dubna, Moscow region, Russia. osipov@thsun1.jinr.ru

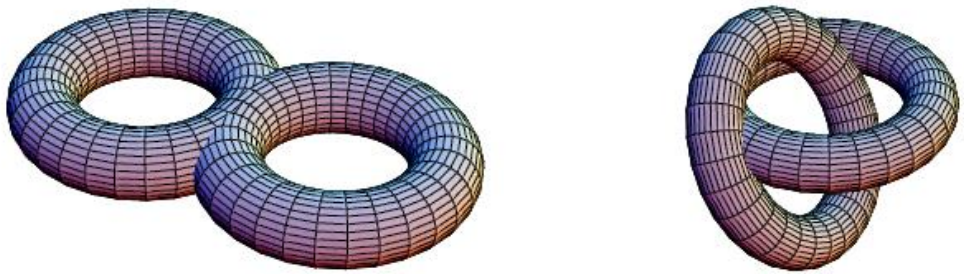

Fig. 5. Exotic configurations

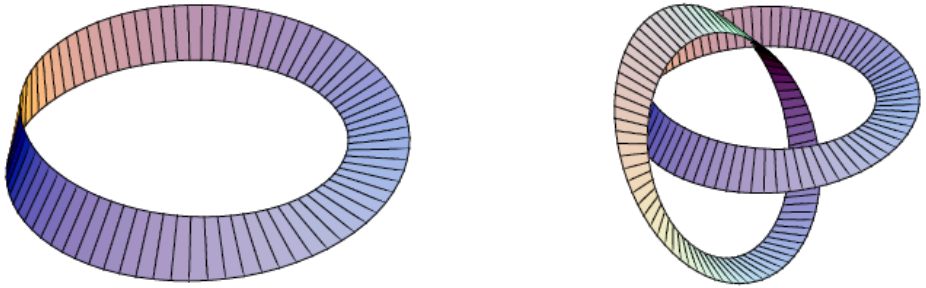

Fig. 6. Möbius stripe (left) and a more exotic configuration

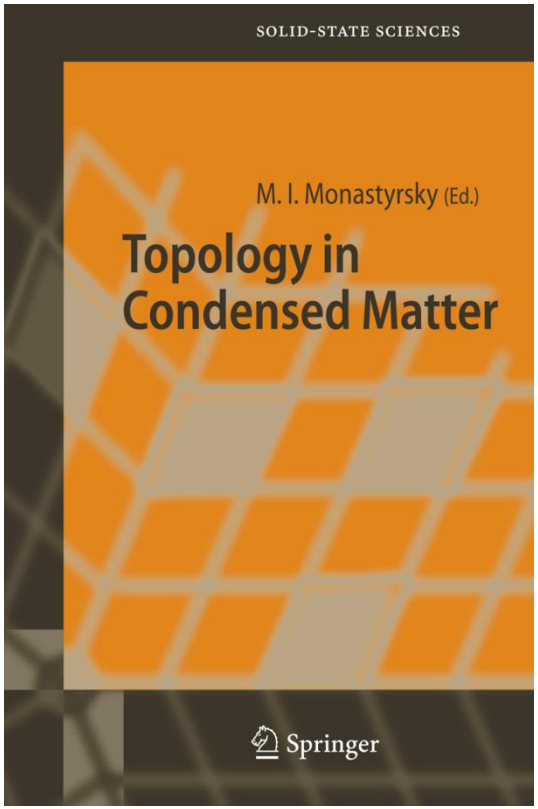

Эксперимент

International weekly journal of science

nature

A Möbius strip of single crystals

Satoshi Tanda*1, Taku Tsuneta*1, Yoshitoshi Okajima*1, Katsuhiko Inagaki*1, Kazuhiko Yamaya*1, Noriyuki Hatakenaka*2

*1 *Department of Applied Physics, Hokkaido University, Sapporo, Hokkaido 060-8628, Japan*
e-mail: tanda@eng.hokudai.ac.jp
*2 *NTT Basic Research Laboratories, Atsugi, Kanagawa 243-0198, Japan*

Reprinted from Nature, Vol. 417, No. 6887, pp. 397–398, 23 May 2002

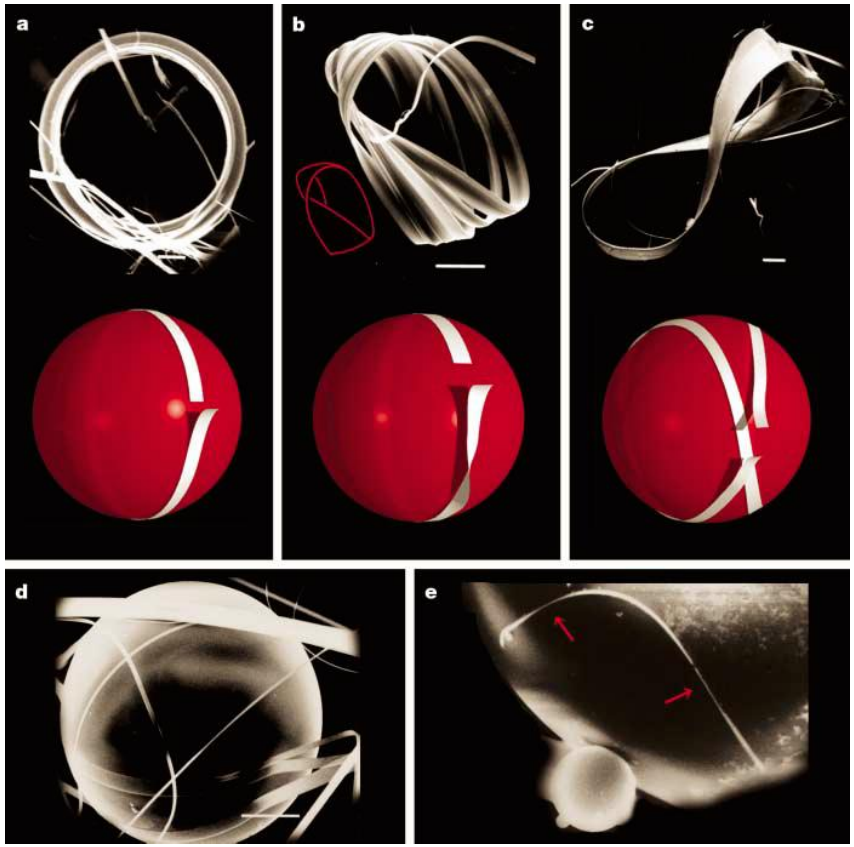

Эксперимент

ELSEVIER

Available online at www.sciencedirect.com
ScienceDirect

Journal of Crystal Growth 297 (2006) 157–160

JOURNAL OF CRYSTAL GROWTH

www.elsevier.com/locate/jcrysgro

Topologically linked crystals

Toru Matsuura[a], Masanori Yamanaka[b], Noriyuki Hatakenaka[c], Toyoki Matsuyama[d], Satoshi Tanda[a,*]

[a]*Department of Applied Physics, Hokkaido University, Sapporo 060-8628, Japan*
[b]*Department of Physics, College of Science and Technology, Nihon University, Tokyo 101-8308, Japan*
[c]*Faculty of Integrated Arts and Sciences, Hiroshima University, Higashi-Hiroshima, 739-8521, Japan*
[d]*Department of Physics, Nara University of Education, Nara 630-8528, Japan*

Received 31 May 2006; received in revised form 21 July 2006; accepted 5 August 2006
Communicated by M. Uwaha
Available online 25 October 2006

Abstract

We discovered a new class of topological crystals, namely linked rings of crystals. Two rings of tantalum triselenide ($TaSe_3$) single crystals were linked to each other while crystal growing. The topology of the crystal form is called a "Hopf link", which is the simplest link involving just two component unknots linked together exactly once. The feature of the crystals is not covered by the conventional crystallography.

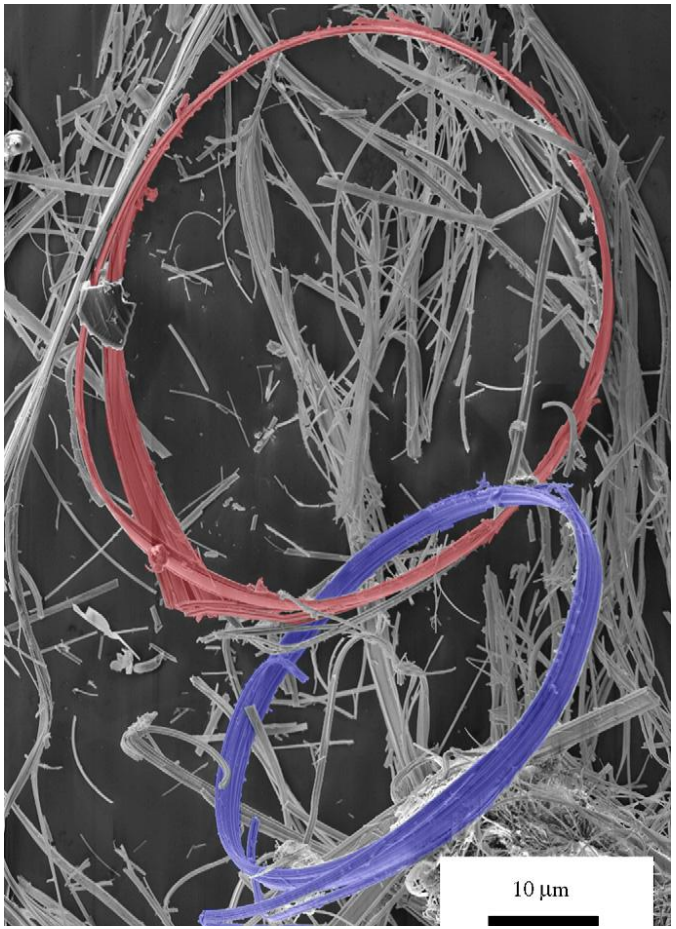

Fig. 1. Scanning electron microscope (SEM) image of linked rings of crystal formed of a compound of tantalum and selenium ($TaSe_3$). The blue and red rings have respective diameters of 46 and 54 μm. The two rings are linked with each other exactly once.

Фуллерены, нанотрубки, конуса, корзинки

Carbon nanostructures

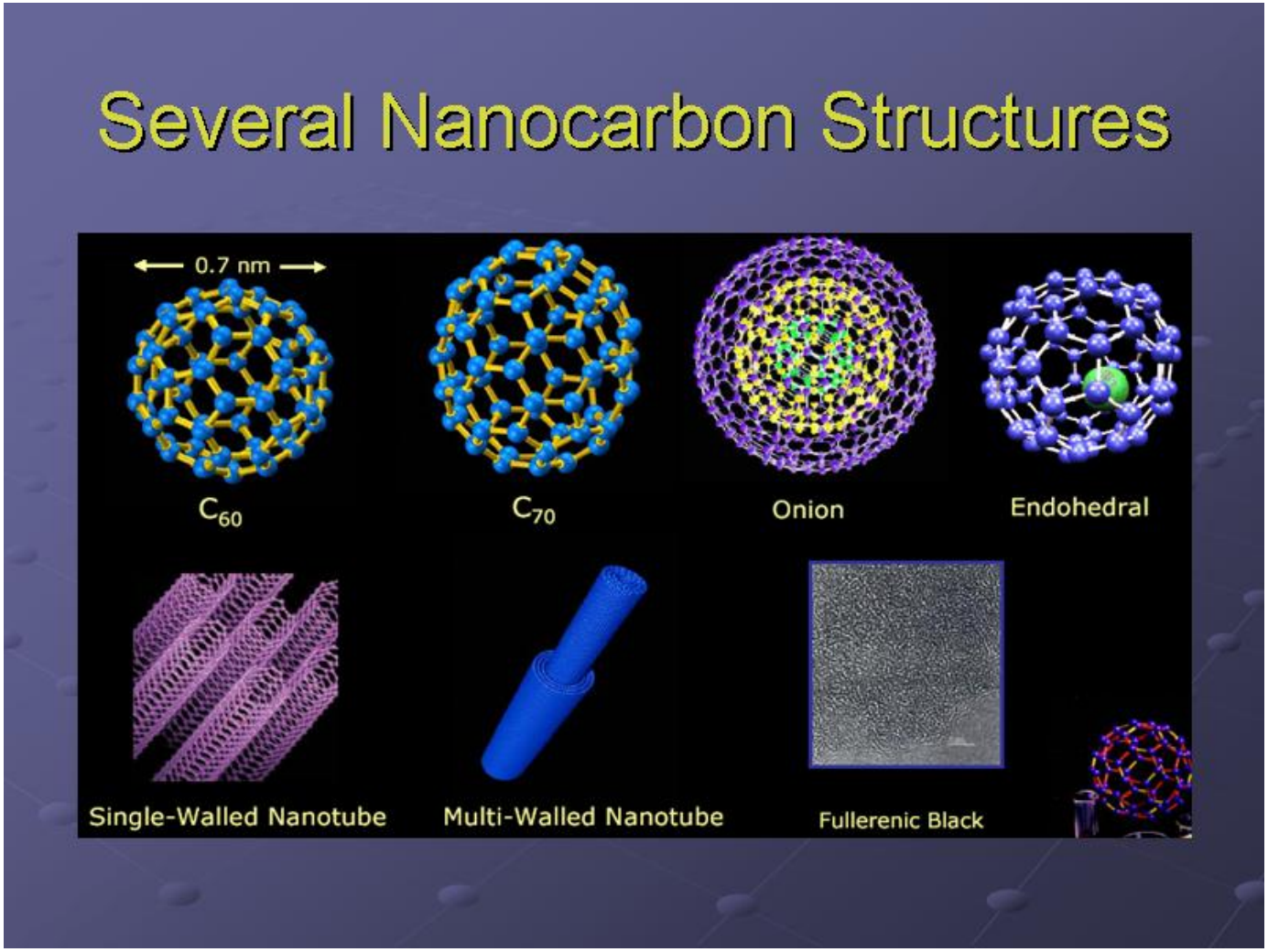

Нобелевская премия по химии (1996)

- English chemist Sir Harold Kroto was corecipient with Richard E. Smalley and Robert F. Curl, Jr., for their joint discovery of the carbon compounds called fullerenes.

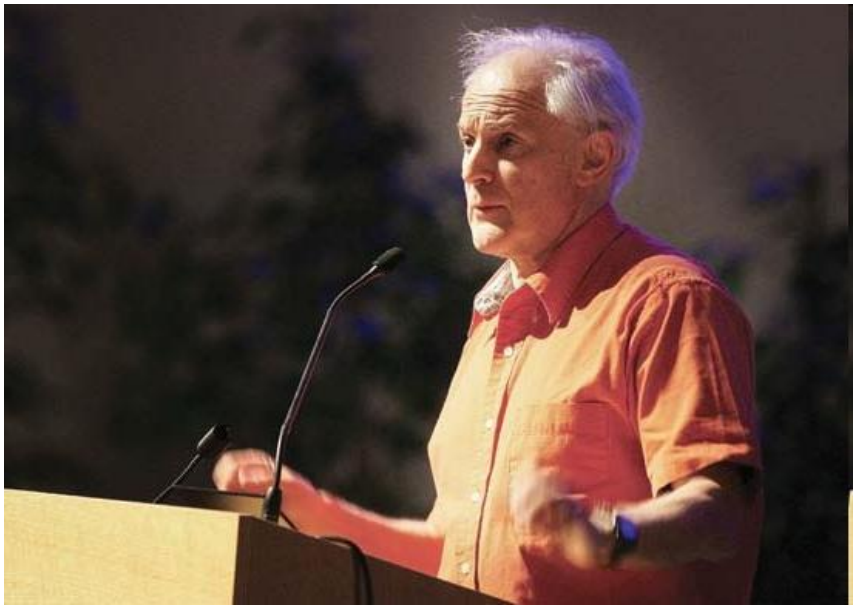

Pentagons (why twelve?)

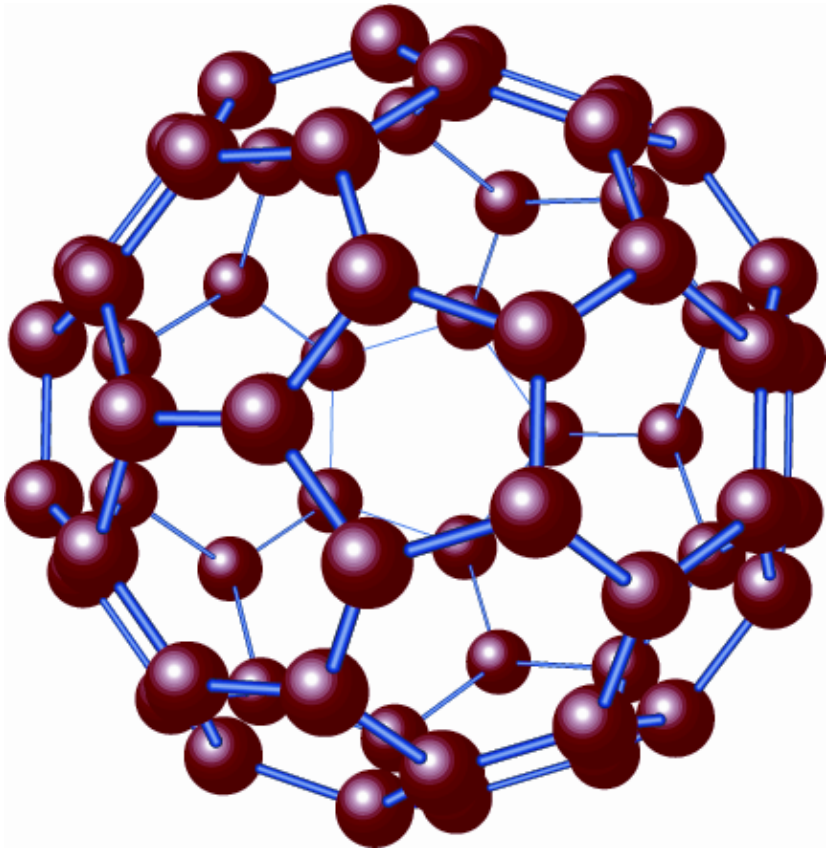

$\Sigma(6-x)n_x=12(1-g)$

Euler’s theorem

Euler's theorem relates the number of vertices, edges and faces of an object

$$\mathbf{...2n_4+n_5-n_7-2n_8... = \sum(6-x)n_x = 12(1-g)}$$

n_x is the number of polygons having x sides, g is the genus. For sphere g=0, n_5=12. Thus, these microcrystals can only be formed by having a total disclination of 4π. According to the geometry of the hexagonal network this means the presence of twelve pentagons (60º disclinations) on the closed hexatic surface.

Important: Disclinations are generic defects in closed carbon structures

Топологические дефекты

Дислокации и дисклинации

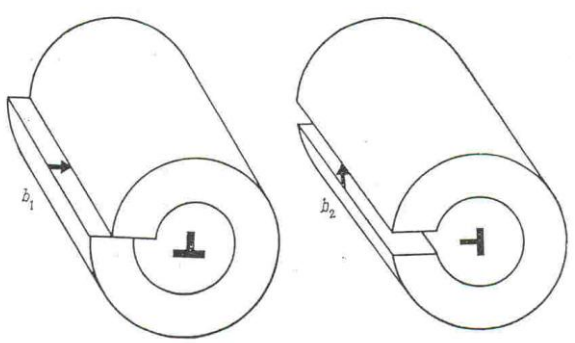

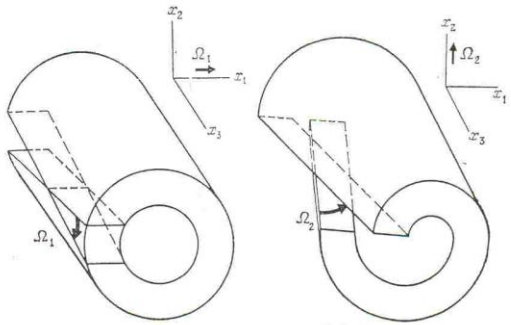

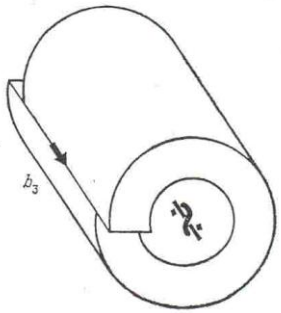

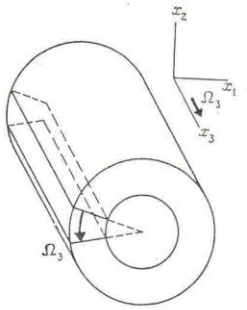

$$\oint\limits_L du_i = \oint\limits_L \frac{\partial u_i}{\partial x_k} dx_k = -b_i.$$

$$\oint\limits_L d\omega_i = \oint\limits_L \frac{\partial \omega_i}{\partial x_k} dx_k = -\Omega_i,$$

$$\vec{u}^P = \vec{u}^+ - \vec{u}^- = \vec{b} + [\vec{\Omega}\vec{R}],$$

$$\vec{\omega} = (1/2) rot \vec{u}$$

Pentagons and disclination buckling transition

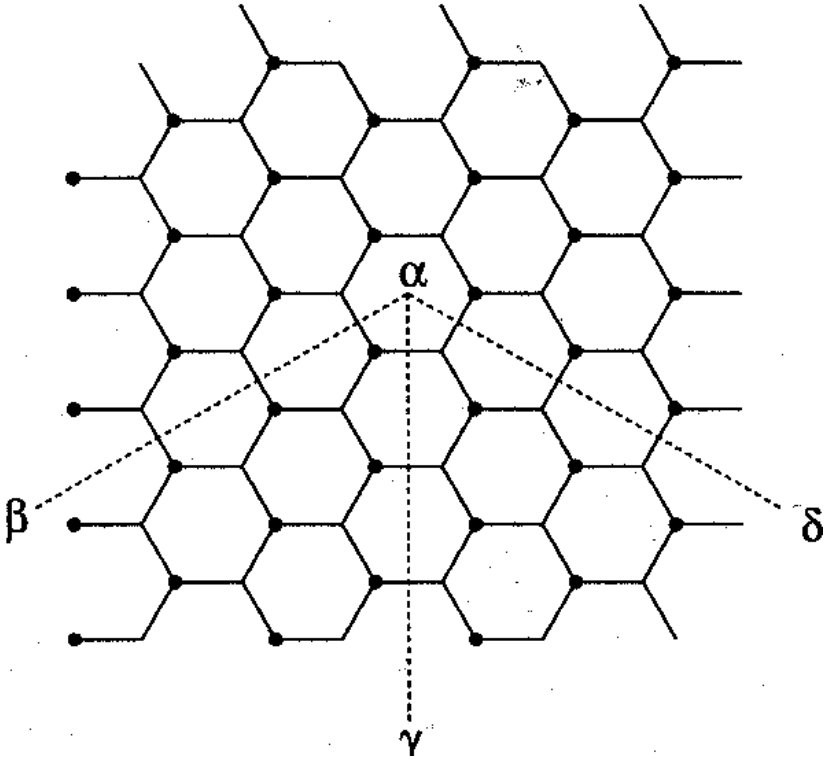

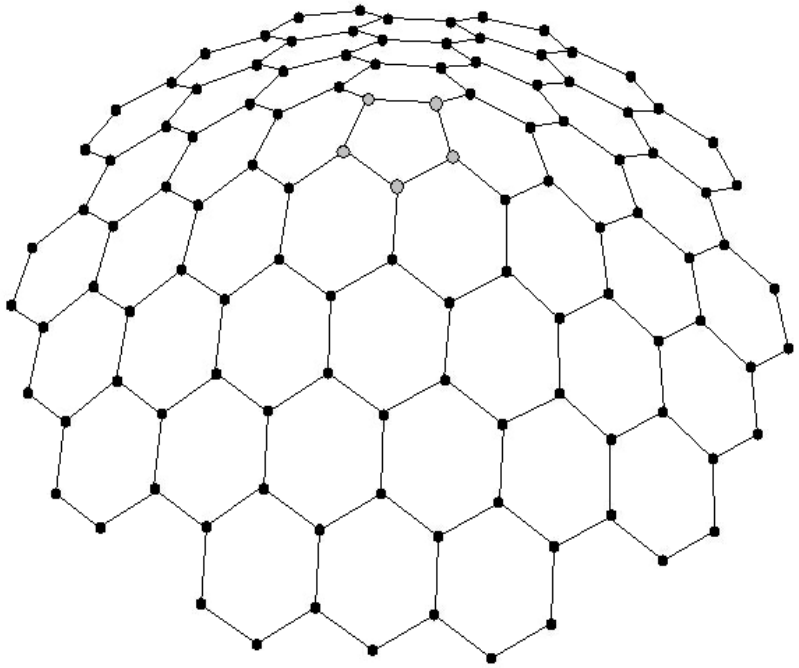

By its nature, the pentagon in a graphite sheet is a topological defect. Actually, fivefold coordinated particles (pentagons) are orientational disclination defects in the otherwise sixfold coordinated triangular lattice.

Defects, Curvature

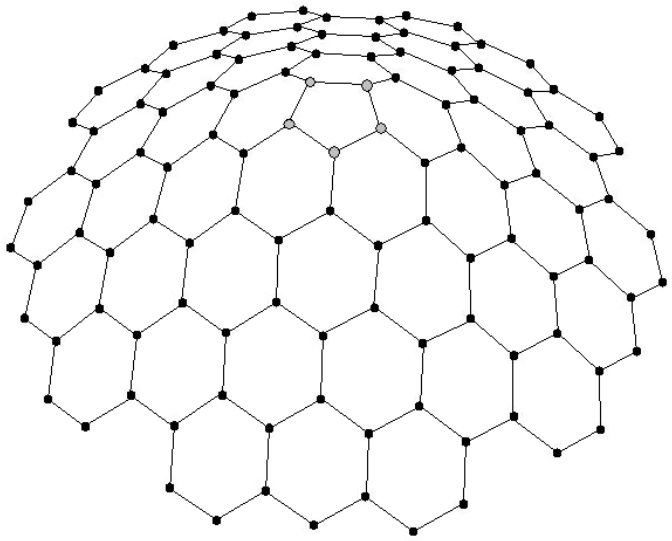

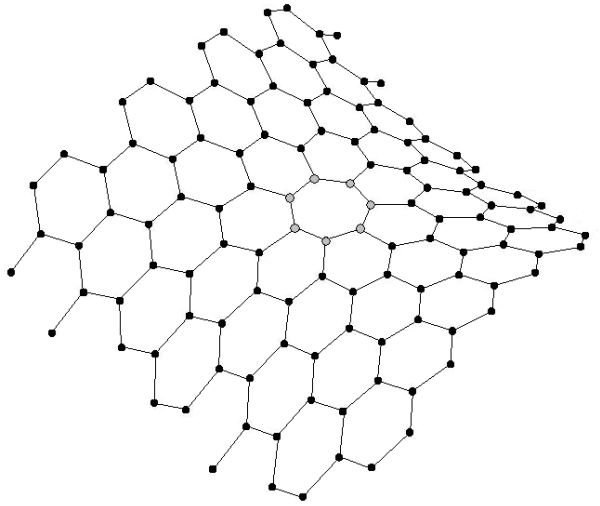

The pentagon (positive curvature) and the heptagon (negative curvature) in the hexagonal graphite lattice

Experimental observation of the pentagon by STM (scanning tunneling microscopy)

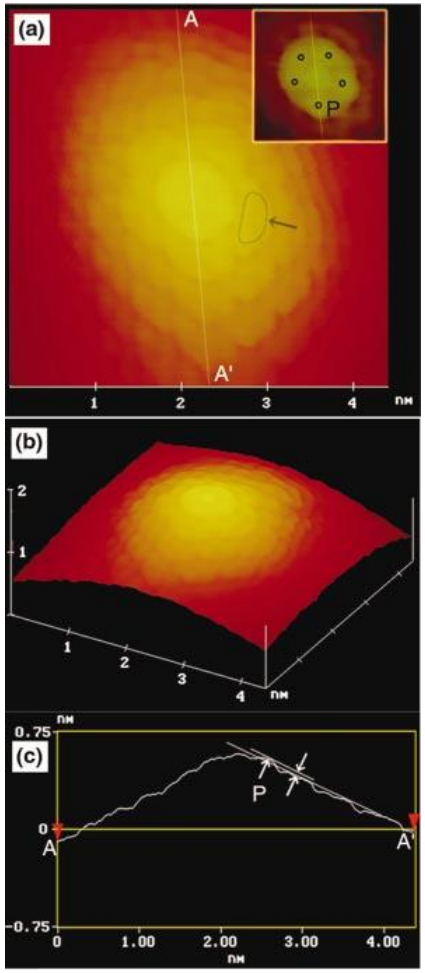

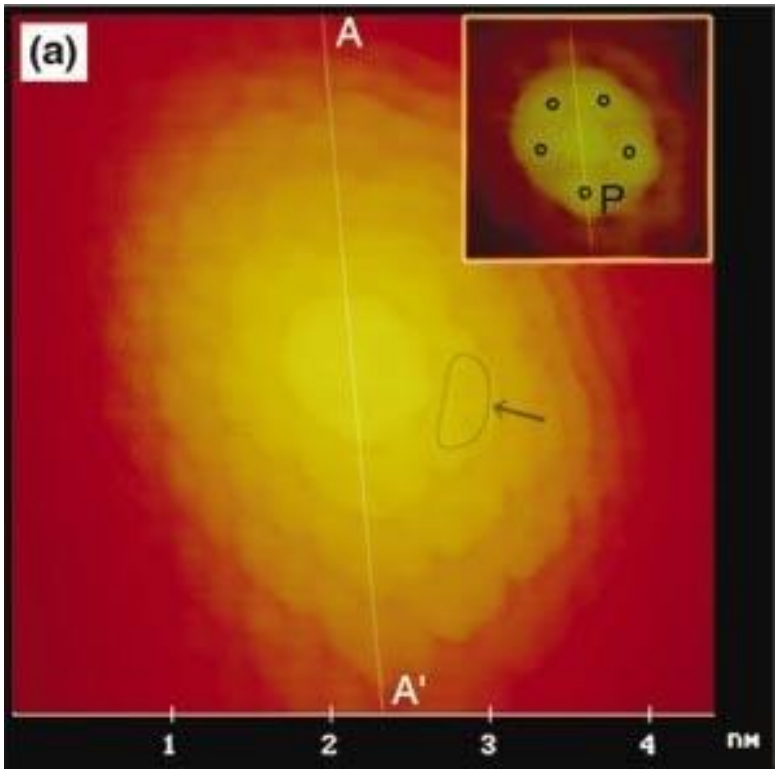

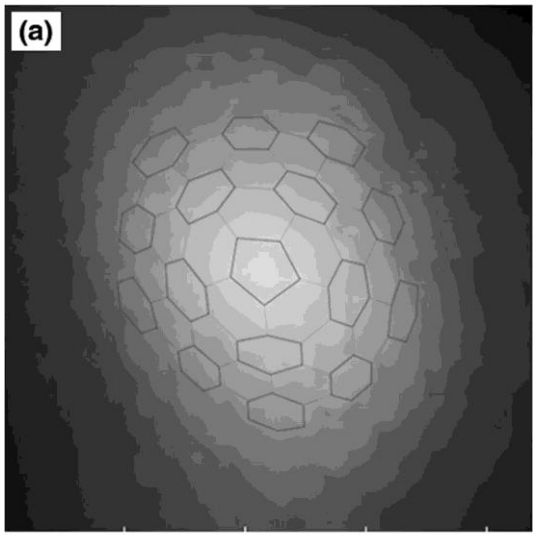

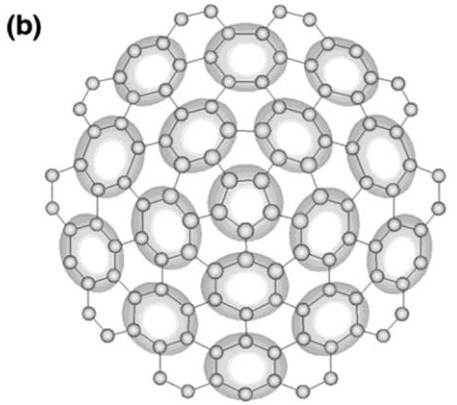

B.An et.al, Appl.Phys.Lett. 78, 3696 (2001): the enhanced charge density localized at each carbon atom in the pentagon was experimentally clarified. Typical images of the conical protuberance by STM: (a) Top view of the apex, (b) Bird's-eye view, (c) Cross section along line AA'. Five bright spots are clearly seen.

Cone geometry

Due to the symmetry of a graphite sheet only five types of cones can be created from a continuous sheet of graphite. The total disclinations of all these cones are multiplies of 60º, corresponding to the presence of a given number (n) of pentagons at the apices.

Important: carbon nanocones with cone angles of 19º, 39º, 60º, 85º, and 113º have been observed in a carbon sample

A. Krishnan et al., Nature (London), **388**, 451 (1997).

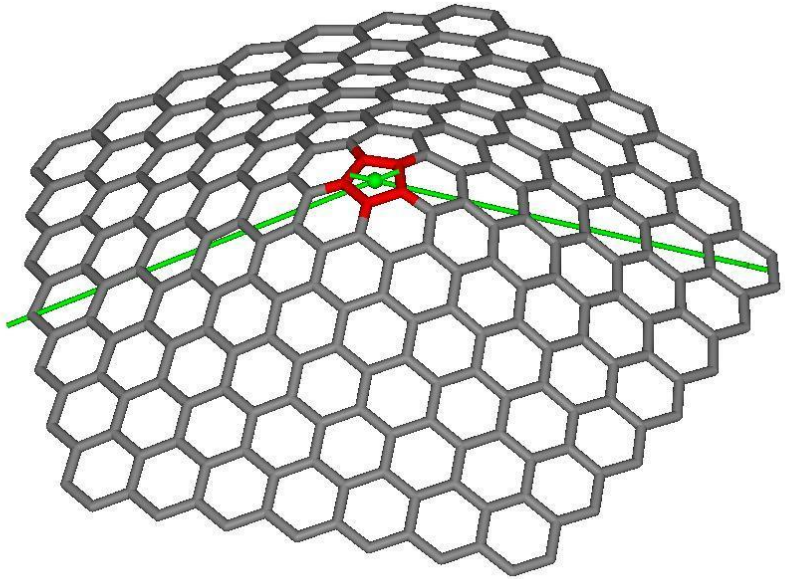

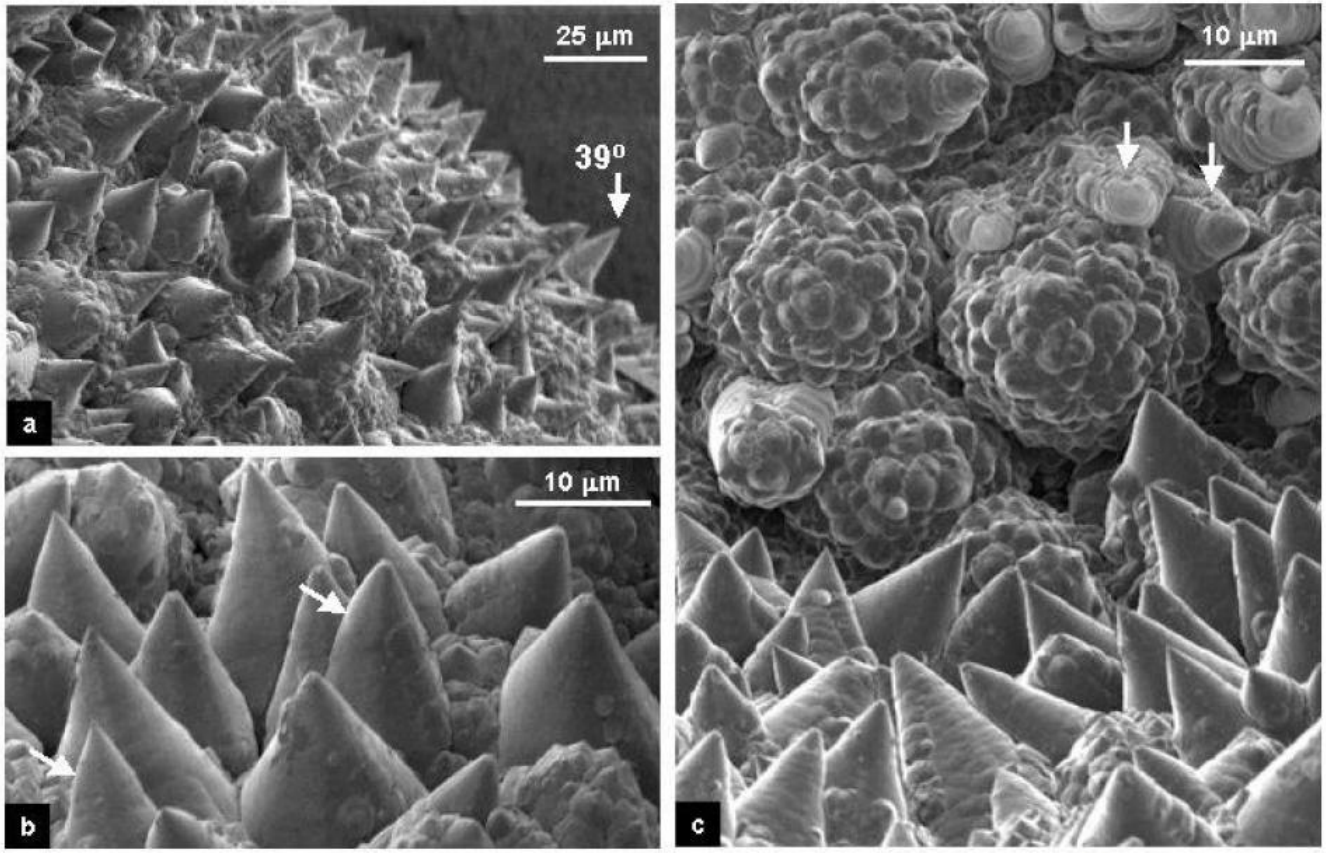

Fig. 2. FESEM images of a cone-covered graphite aggregate. (a) Low-magnification image showing complete coverage of the aggregate surface with conical structures. A ~39° cone is marked by an arrow. (b) Higher magnification image of the sample showing a variety of large cones with different apex angles and sharp and blunt tips. Arrows show changes in the apex angle. (c) Close up view of two surfaces which are almost perpendicular and show different cone morphologies – large cones on one surface and globular (artichoke-like) structures on the other. The latter ones are clusters of large-angle cones. Arrows show some of the cones that are ripped on the side

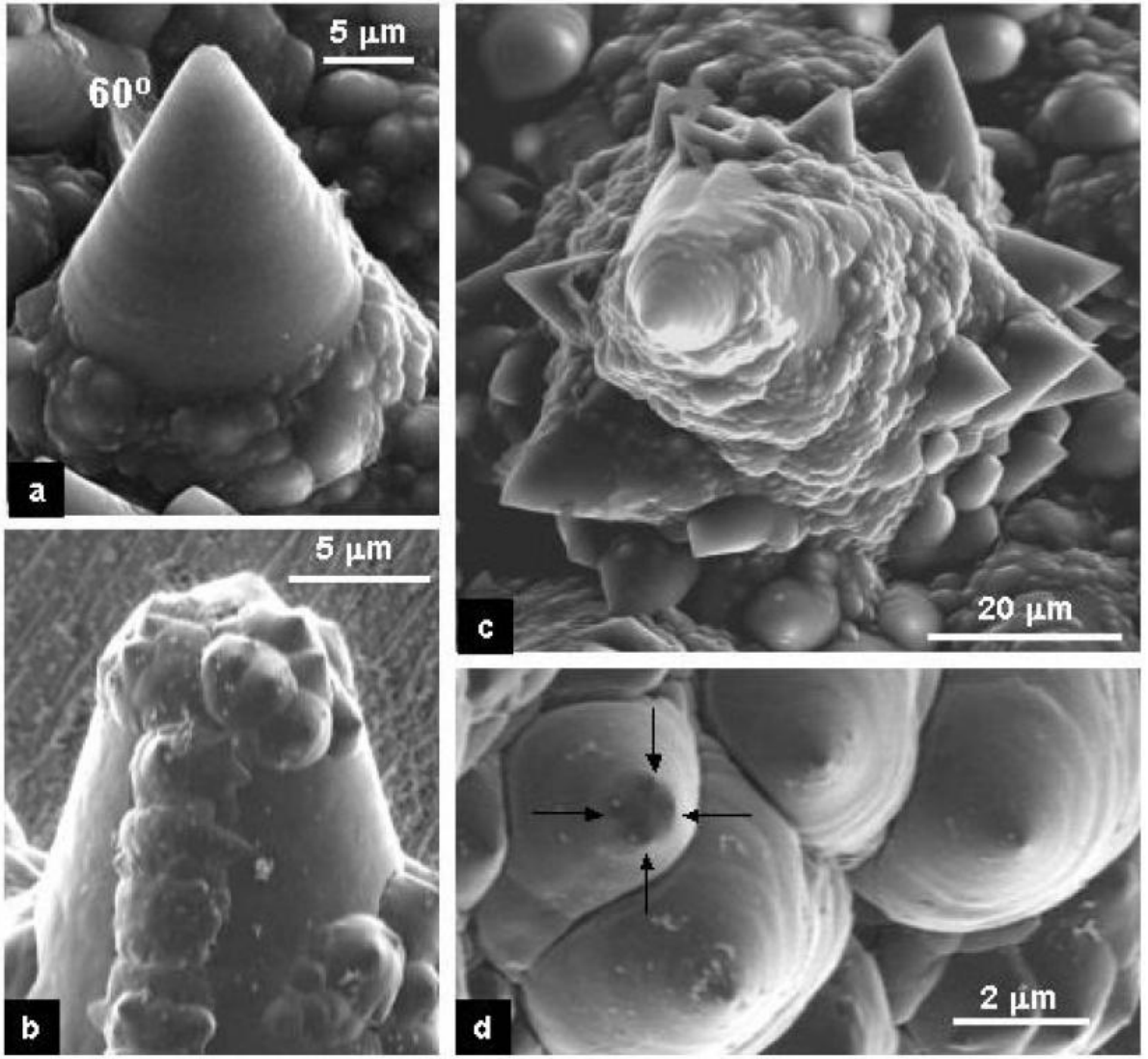

Fig. 3. Typical cone morphologies. (a) SEM image of a cone with a 60° apex angle, the most common apex angle. The slightly uneven surface of the cone suggests layer growth. (b) FESEM and (c) SEM images of large cones with numerous smaller cones growing on their surface. Smaller cones covering surfaces of large cones have a broad distribution of shapes, but large apex angles prevail (c). (d) FESEM image of four cones having sharp and broad tips (multiple tips are marked by arrows). The cones are oriented to reveal their circular cross sections around the tips and layered growth (ripples).

A presence of sharp resonant states in the region close to the Fermi energy

J.-C. Charlier and G.-M. Rignanese, Phys. Rev.Lett. 86, 5970 (2001)

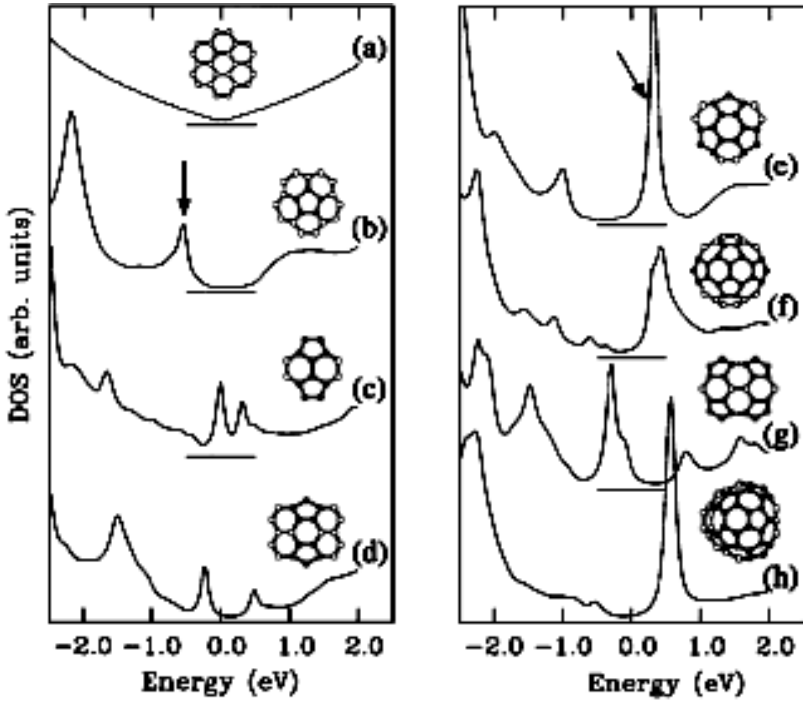

Computed tight-binding LDOS for a single graphene layer (a), and nanocones with one (b), two (c) and (d), three (e), four (f) and (g), and five (h) pentagons, respectively. The Fermi level is at zero energy.

The strength and the position of these states with respect to the Fermi level was found to depend sensitively on the number and the relative positions of the pentagons constituting the conical tip. In particular, a prominent peak which appears just above the Fermi level was found for the nanocone with three symmetrical pentagons (which corresponds to a 60˚ opening angle or, equivalently, to 180˚ disclination).

Nanohorns

Source: S. Berber et al., Phys.Rev.B 62, R2291 (2000)

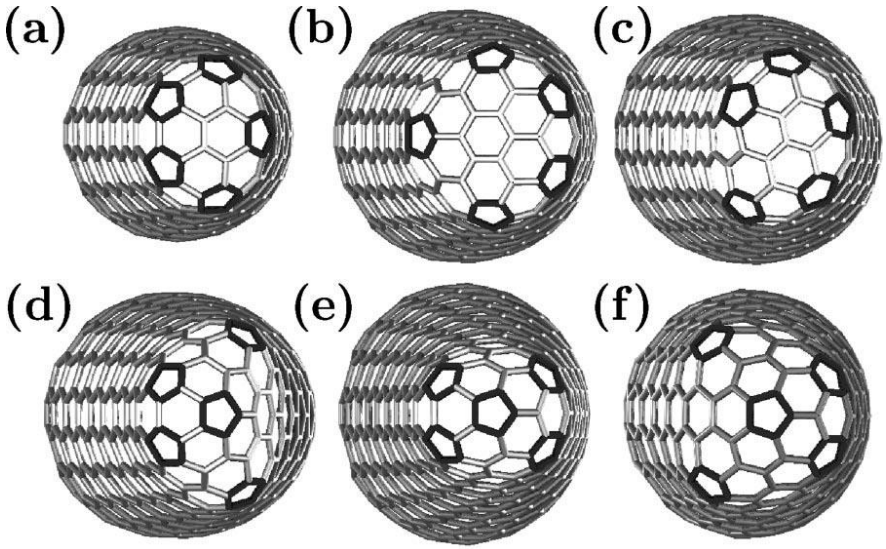

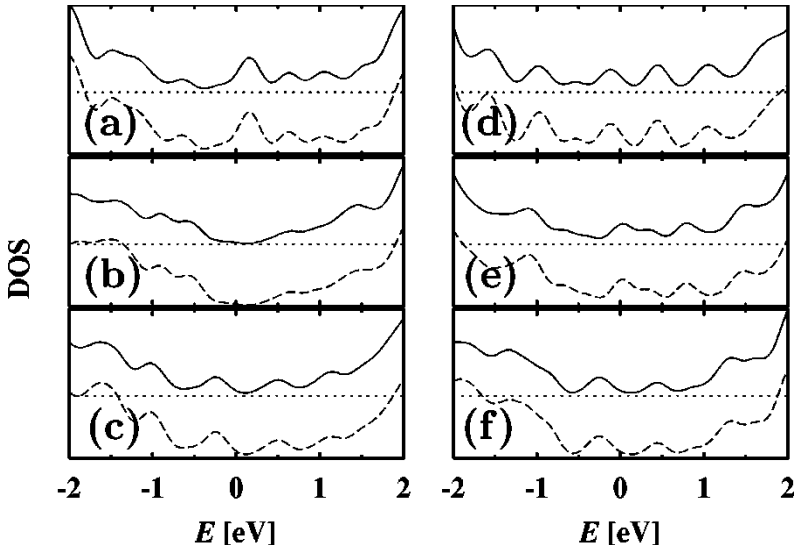

Carbon nanohorn structures with a total disclination angle of 5(π/3), containing five isolated pentagons at the terminating cap. Structures (a)–(c) contain all pentagons at the conical ‘‘shoulder,’’ whereas structures (d)–(f) contain a pentagon at the apex.

Graphite plane

J.C. Slonczewski and P.R. Weiss, Phys.Rev. 109, 272 (1958)

Real space

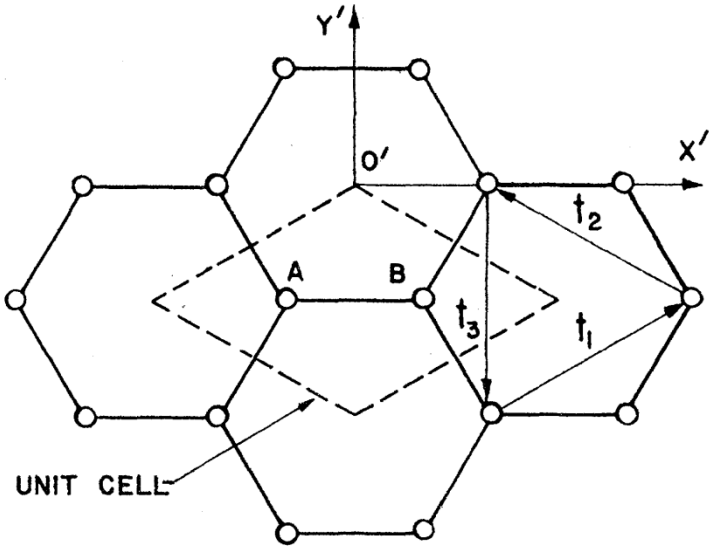

Reciprocal space

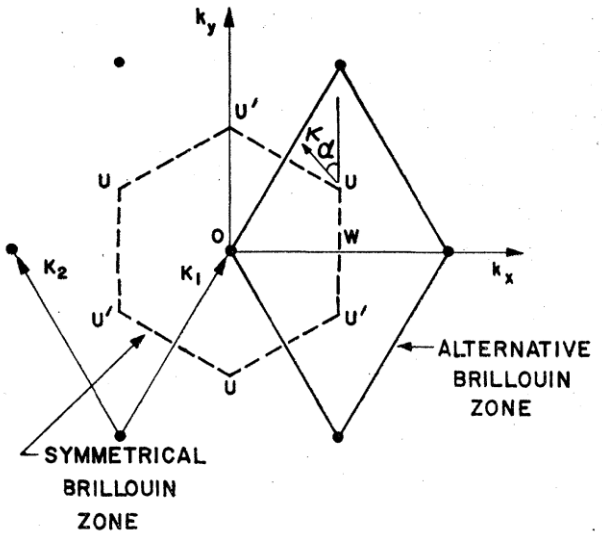

Important:

- there are two atoms per unit cell;
- there are to generate Bloch eigenstates at the Fermi point.

Lattice, spectrum

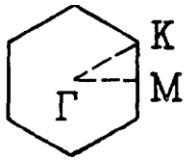

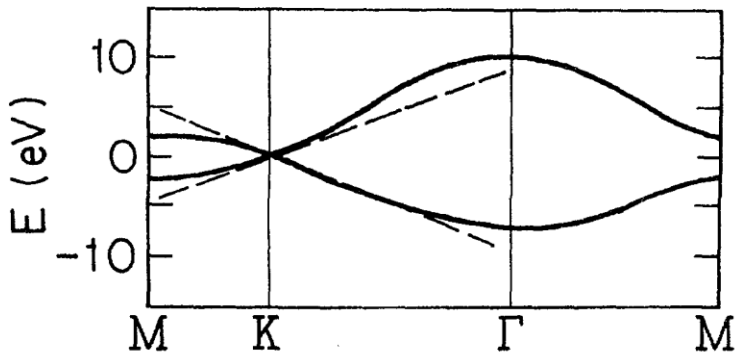

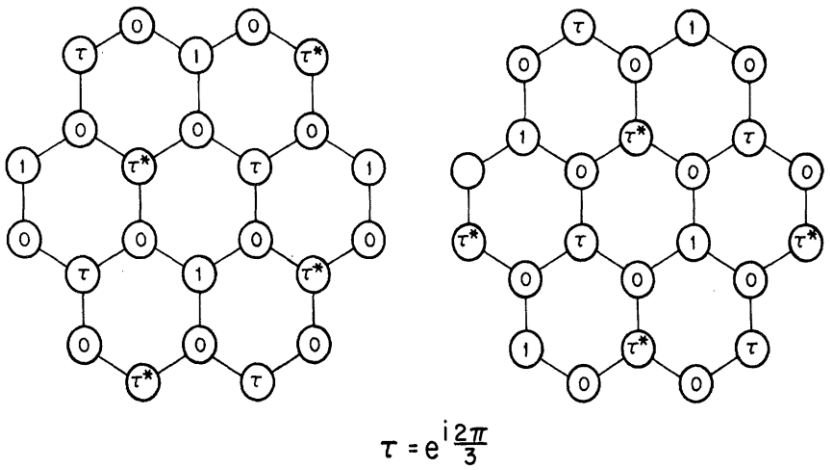

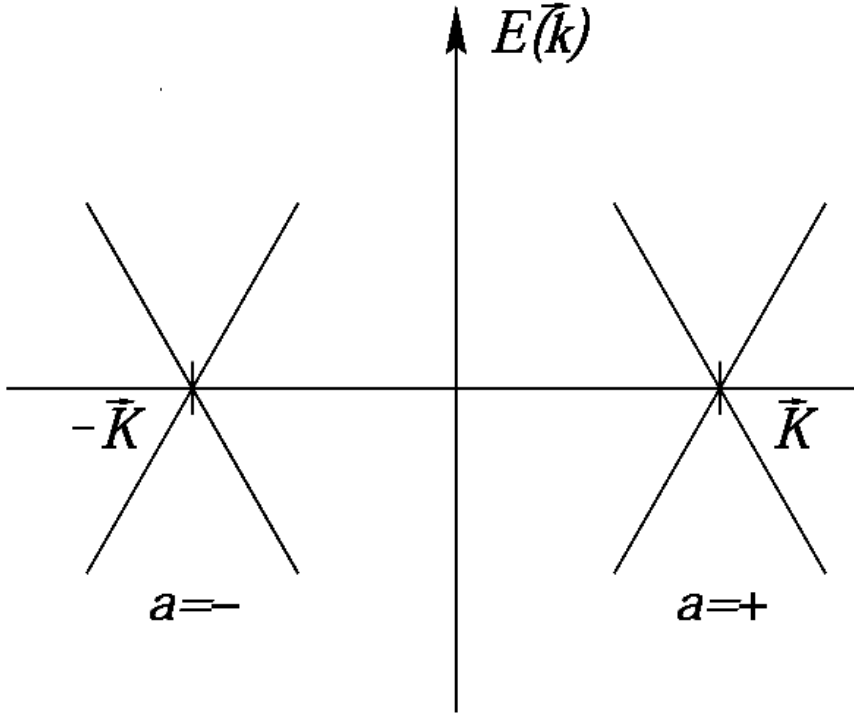

Energy-band structure of the bands of a two-dimensional graphite layer.

Two degenerate eigenstates which provide the basis set for the **kp** trial wave function.

Dirac equation

Step1: the effective-mass approximation, which is equivalent to the kp expansion about the K point in the Brillouin zone

$$\Psi(\boldsymbol{k},\boldsymbol{r}) = f_1(\boldsymbol{k}')e^{i\boldsymbol{k}'\boldsymbol{r}}\Psi_1^S(\boldsymbol{K},\boldsymbol{r}) + f_2(\boldsymbol{k}')e^{i\boldsymbol{k}'\boldsymbol{r}}\Psi_2^S(\boldsymbol{K},\boldsymbol{r})$$

Step2: put it in the Schroedinger equation and diagonalize the secular equation for functions f_i. As a result,

$$\psi = \begin{pmatrix} f_1 \\ f_2 \end{pmatrix}$$

$$-i\sigma^\mu \partial_\mu \psi(\boldsymbol{r}) = E\psi(\boldsymbol{r})$$

The most important fact is that the electronic spectrum of a single graphite plane linearized around the corners of the hexagonal Brillouin zone coincides with that of the Dirac equation in (2+1) dimensions

DOS in 2D

$$DoS(E) = \frac{gV}{4\pi^2} \oint_{\epsilon=E} \frac{dS}{|grad_k \epsilon(\vec{k})|}.$$

g = 4 –degeneracy of electronic states

For linear (Dirac-type) spectrum

$$DoS(E) = \frac{gV|E|}{2\pi},$$

Linear in energy E

Local DOS for arbitrary surface

$$LDoS(E, x) = \Sigma_k |\psi_k(x)|^2 \delta(\epsilon(k) - E)$$

Педагогический пример

Defects in flexible membranes with crystalline order

H. S. Seung and David R. Nelson
Lyman Laboratory of Physics, Harvard University, Cambridge, Massachusetts 02138
(Received 3 March 1988)

We study isolated dislocations and disclinations in flexible membranes with internal crystalline order, using continuum elasticity theory and zero-temperature numerical simulation. These defects are relevant, for instance, to lipid bilayers in vesicles or in the L_β phase of lyotropic smectic liquid crystals. We first simulate defects in flat membranes, obtaining numerical results in good agreement with plane elasticity theory. Disclinations and dislocations eventually exhibit a buckling transition with increasing membrane radius. We generalize the continuum theory to include such buckled defects, and solve the disclination equations in the inextensional limit. The critical radius at which buckling starts to screen out internal elastic stresses is determined numerically. Computer simulation of buckled defects confirms predictions of the disclination energies and gives evidence for a finite dislocation energy.

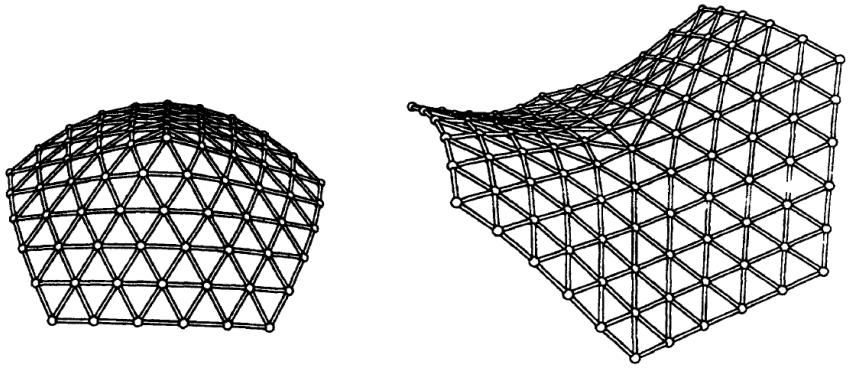

(a) (b)

FIG. 5. (a) Buckled positive disclination ($K_0/\tilde{\kappa}=2000$). (b) Buckled negative disclination ($K_0/\tilde{\kappa}=2000$).

$$\kappa \nabla^4 f = \frac{\partial^2 \chi}{\partial y^2}\frac{\partial^2 f}{\partial x^2} + \frac{\partial^2 \chi}{\partial x^2}\frac{\partial^2 f}{\partial y^2} - 2\frac{\partial^2 \chi}{\partial x\,\partial y}\frac{\partial^2 f}{\partial x\,\partial y}\ , \tag{4.10a}$$

$$\frac{1}{K_0}\nabla^4 \chi + \frac{\partial^2 f}{\partial x^2}\frac{\partial^2 f}{\partial y^2} - \left[\frac{\partial^2 f}{\partial x\,\partial y}\right]^2 = \sum_\alpha s_\alpha \delta(\mathbf{r}-\mathbf{r}_\alpha) + \sum_\beta b_i^\beta \epsilon_{ik}\partial_k \delta(\mathbf{r}-\mathbf{r}_\beta)\ . \tag{4.10b}$$

For a defect-free membrane, the δ-function terms vanish, and we are left with the von Kármán equations for large deflections of thin plates.[19] These coupled nonlinear partial differential equations are "very complicated, and cannot be solved exactly, even in very simple cases."[7]

For an isolated positive disclination at the origin, we assume rotational symmetry and write Eqs. (4.10) away from the disclination core as

$$\kappa \nabla^4 f = \frac{1}{r}\frac{d}{dr}\left[\frac{d\chi}{dr}\frac{df}{dr}\right], \tag{4.11a}$$

$$\frac{1}{K_0}\nabla^4 \chi + \frac{1}{2r}\frac{d}{dr}\left[\frac{df}{dr}\right]^2 = 0, \tag{4.11b}$$

where

$$\nabla^2 = \frac{1}{r}\frac{d}{dr} r \frac{d}{dr} .$$

It is not difficult to guess a trial solution of these equations,

$$\chi = -\kappa \ln\left[\frac{r}{a}\right], \tag{4.12a}$$

$$f = \pm\left[\frac{s}{\pi}\right]^{1/2} r . \tag{4.12b}$$

Although it would appear that we have found an exact solution, comparison with the original form of the von Kármán equations (4.8) reveals that (4.12) is not a true solution because the left-hand side of Eq. (4.8b) is proportional to $\nabla^2\delta(\mathbf{r})$, while the right-hand side vanishes. If we attempt to bypass this issue by deleting a small disk of material around the origin, we create an inner boundary on which σ_{rr} and $\sigma_{r\phi}$ must vanish. One can easily calculate from the expression (4.12a) for χ that σ_{rr} behaves like $1/r^2$, so the inner boundary condition is badly violated if we excise a small disk.

IOP PUBLISHING JOURNAL OF PHYSICS: CONDENSED MATTER

J. Phys.: Condens. Matter **22** (2010) 395502 (11pp) doi:10.1088/0953-8984/22/39/395502

Electronic properties of disclinated flexible membrane beyond the inextensional limit: application to graphene

E A Kochetov[1], V A Osipov[1] and R Pincak[1,2]

Actually, a general solution must include a homogeneous term

$$\chi_0 = -\log\frac{r}{r_0} + q\frac{r}{r_0}$$

The stress tensor takes the form

$$\sigma_{rr} = -\frac{1}{r^2} + \frac{q}{rr_0}$$

$\sigma_{rr}(r = r_0) = \sigma_0$ yields $q = 1 + \sigma_0 r_0^2$

The stretching energy of the membrane

$$E_s \propto \frac{\kappa^2 q^2}{K_0 r_0^2}\log\frac{R}{r_0}$$

Генерация метрики калибровочным полем

1. Поверхность вкладываем в R3 $R^i_{(0)}(x^1, x^2)$

2. Метрика $$g^{(0)}_{ab} \equiv (g_{\Sigma_0})_{ab} = \partial_a \vec{R}_{(0)} \cdot \partial_b \vec{R}_{(0)}$$

инвариантна относительно вращений вектора R (группы SO(3))

3. Требуем инвариантность относительно локальных вращений – генерируется новая метрика

$$g_{ab} = g^{(0)}_{ab}(\vec{W}^{(0)}) = \nabla_a \vec{R}_{(0)} \cdot \nabla_b \vec{R}_{(0)} = \partial_a \vec{R}_{(0)} \cdot \partial_b \vec{R}_{(0)} + \partial_a \vec{R}_{(0)}[\vec{W}^{(0)}_b, \vec{R}_{(0)}] + \partial_b \vec{R}_{(0)}[\vec{W}^{(0)}_a, \vec{R}_{(0)}]$$
$$+ (\vec{W}^{(0)}_a \vec{W}^{(0)}_b)\vec{R}^2_{(0)} - (\vec{W}^{(0)}_a \vec{R}_{(0)})(\vec{W}^{(0)}_b \vec{R}_{(0)}).$$

Пример

$$W_\mu^{(0)i=1,2} = 0 \text{ and } W_\mu^{(0)i=3} = W_\mu^{(0)}$$

$$W_x^{(0)} = \nu y/r^2,\ W_y^{(0)} = -\nu x/r^2,\ r = \sqrt{x^2+y^2} \neq 0$$

$$\oint_C W_a^{(0)} dx^a = -2\pi\nu \neq 0$$

Плоскость

$$(r,\varphi) \to (r\cos\varphi,\ r\sin\varphi, 0), \quad 0 < r < \infty,\ 0 \leq \varphi < 2\pi.$$

плюс

$$W_r^{(0)} = 0,\ W_\varphi^{(0)} = -\nu$$ дает метрику конуса

$$g_{rr} = 1, \qquad g_{\varphi\varphi} = \alpha^2 r^2, \qquad g_{r\varphi} = g_{\varphi r} = 0$$

Back to the Dirac equation

The Dirac equation on an arbitrary surface in the presence of the gauge field a_b and the external magnetic field with the vector potential A_b is written as

$$\mathrm{i}\gamma^{\alpha} e_{\alpha}^{b}[\nabla_b - \mathrm{i}a_b - \mathrm{i}A_b]\psi = E\psi$$

with $\nabla_b = \partial_b + \Omega_b$

Geometrical characteristics

Covariant derivative

$$\nabla_\mu = \partial_\mu + \Omega_\mu$$

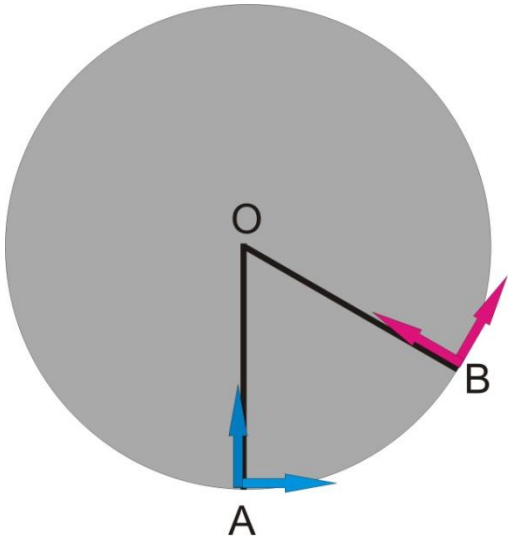

Spin connection term

$$\Omega_\mu = (1/8)\omega^{\alpha}{}_{\mu}{}^{\beta}[\sigma_\alpha, \sigma_\beta]$$

Spin connection coefficients:

$$(\omega_\mu)^{ab} = e^a_\nu(\partial_\mu e^{\nu b} - \Gamma^\nu_{\mu\chi} e^{\chi b}) = -(\omega_\mu)^{ba}$$

Metric connection coefficients

$$\Gamma^\nu_{\mu\lambda} = \frac{g^{\nu\chi}}{2}(\partial_\mu g_{\chi\lambda} + \partial_\lambda g_{\chi\mu} - \partial_\chi g_{\mu\lambda})$$

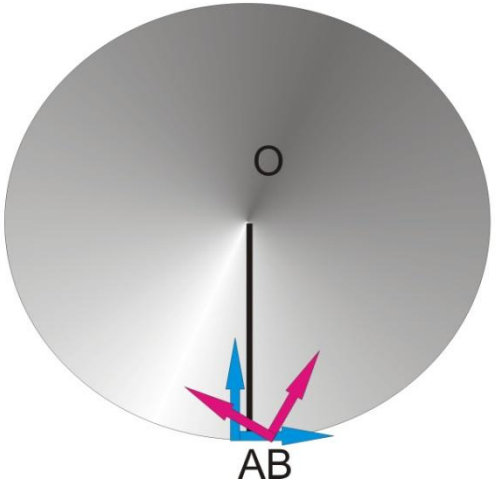

Elastic membrane

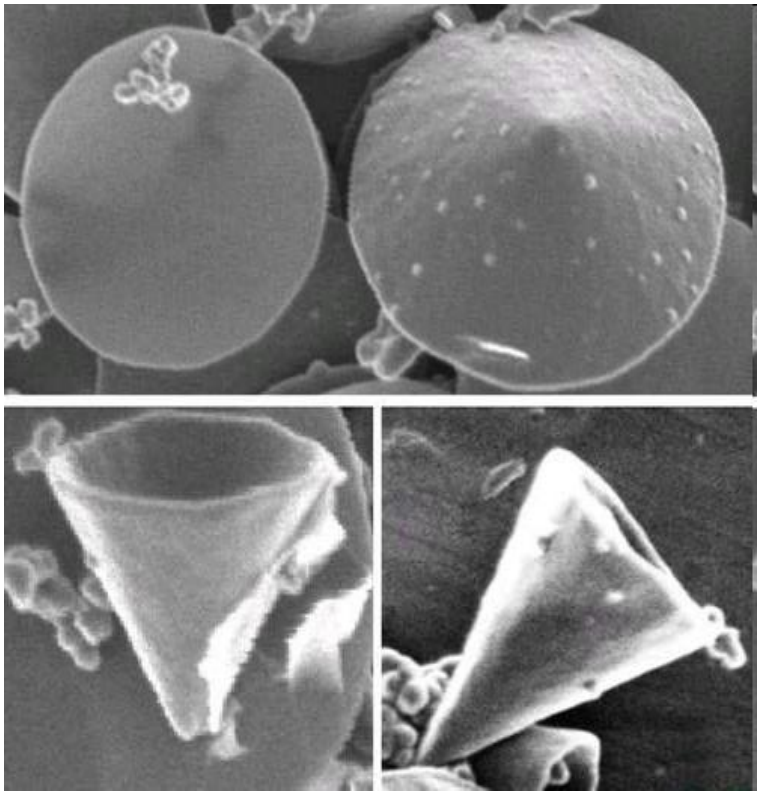

- The principally new model was formulated and applied to study the structure of the low energy electronic states of flexible graphene membrane with a topological defect.

- E.A. Kochetov, V.A. Osipov, and R. Pincak, *J*. Phys.: Condens. Matter **22** (2010)

SEM images of a carbon disk (top left image) and free-standing hollow carbon nanocones produced by pyrolysis of heavy oil

Schematic densities of states for a small patch near the apex of a cone at zero magnetic field and $K_0 \rightarrow$ infinity

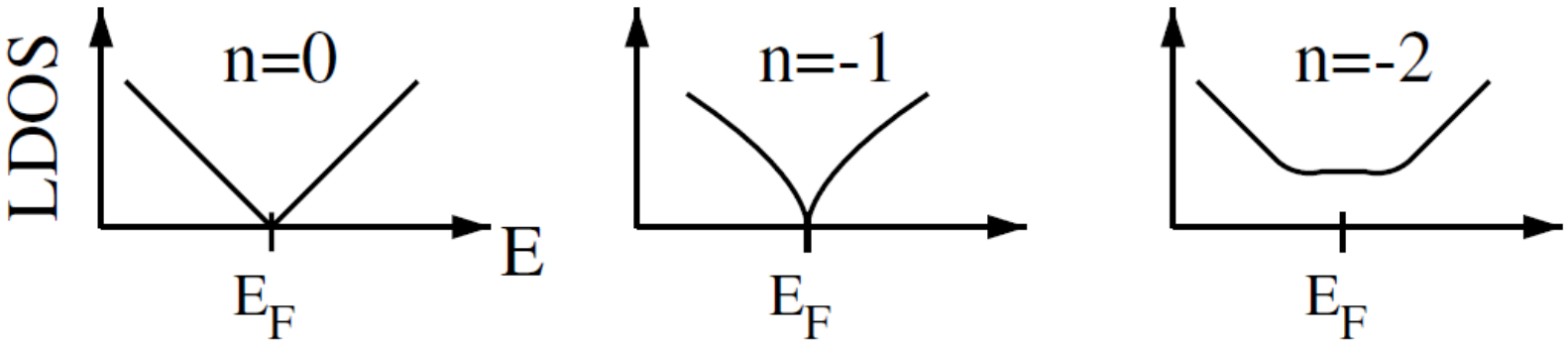

However, a cone with a point-like apex is a mathematical abstraction since in a real situation the media has a finite stiffness, which would inevitably result in a certain smearing of a conical singularity.

Nanocones: another geometry

Upper half of a two-sheet hyperboloid

$$(\chi, \varphi) \to (a \sinh \chi \cos \varphi, a \sinh \chi \sin \varphi, c \cosh \chi)$$

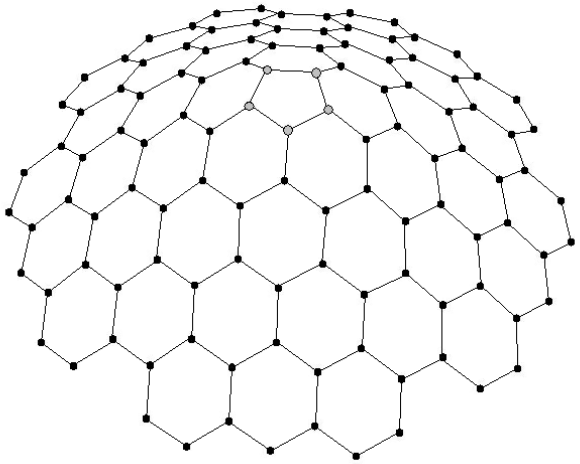

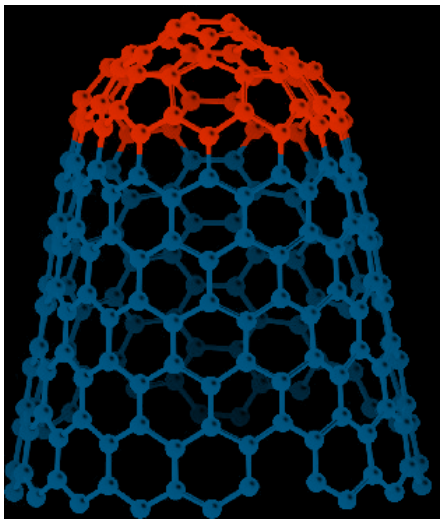

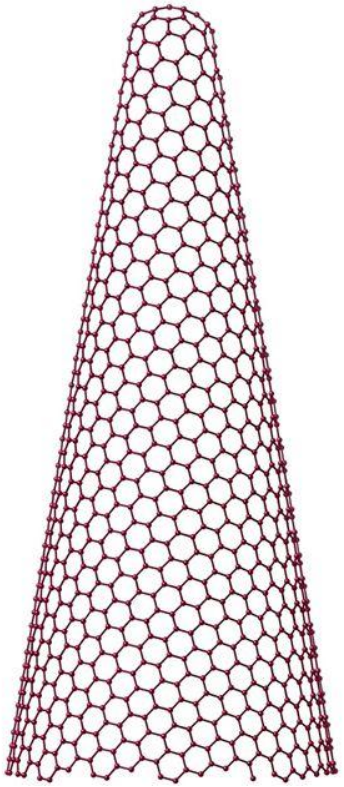

is suitable for the description of cone-like structures with pentagons situated at a smoothed apex. The most appropriate model for nanohorns with five pentagons at the tip.

However, one cannot incorporate finite elasticity into the theory by simply replacing a cone by a smooth surface that asymptotically approaches a cone far away from the origin. This would simply eliminate the defect. To illustrate this, consider an upper half of a hyperboloid as an embedding

$$(\xi, \varphi) \to (a \sinh\xi \cos\varphi, a \sinh\xi \sin\varphi, c \cosh\xi)$$

$$0 \leqslant \xi < \infty, \quad 0 \leqslant \varphi < 2\pi.$$

The components of the induced metric can be written as

$$g_{\xi\xi} = a^2 \cosh^2\xi + c^2 \sinh^2\xi, \qquad g_{\varphi\varphi} = a^2 \sinh^2\xi$$

$$g_{\varphi\xi} = g_{\xi\varphi} = 0,$$

which gives for the spin connection coefficients

$$\omega_{\xi}^{12} = \omega_{\xi}^{21} = 0,$$

$$\omega_{\varphi}^{12} = -\omega_{\varphi}^{21} = \left[1 - \frac{a\,\cosh\xi}{\sqrt{g_{\xi\xi}}}\right] =: \omega(\xi)$$

Since $\omega(\xi)$ goes to zero as $\xi \to 0$ a circulation of that field over a loop encircling the origin gives a flux which tends to zero as the counter shrinks to zero:

$$\lim_{\epsilon \to 0} \oint_{C_\epsilon} \omega_{\varphi}^{12}\, \mathrm{d}\varphi = 0,$$

To incorporate flux we suggest the following metrics

$$g_{\xi\xi} = a^2 \cosh^2 \xi + c^2 \sinh^2 \xi,$$

$$g_{\varphi\varphi} = a^2 \alpha^2 \sinh^2 \xi, \qquad g_{\varphi\xi} = g_{\xi\varphi} = 0,$$

with $\alpha = 1 - \nu$

This metric generates the spin connection term

$$\omega_{\varphi}^{12} = -\omega_{\varphi}^{21} = \left[1 - \frac{a\alpha \cosh \xi}{\sqrt{g_{\xi\xi}}}\right] = \omega_{\alpha}(\xi)$$

and now

$$\lim_{\epsilon \to 0} \oint_{C_\epsilon} \omega_{\varphi}^{12} \, \mathrm{d}\varphi = 2\pi \nu.$$

$$\partial_\xi \tilde{u} - \frac{(j+1/2-a_\varphi+A_\varphi)}{\alpha}\sqrt{\coth^2\xi+\eta}\,\tilde{u} = \tilde{E}\tilde{v},$$

$$-\partial_\xi \tilde{v} - \frac{(j+1/2-a_\varphi+A_\varphi)}{\alpha}\sqrt{\coth^2\xi+\eta}\,\tilde{v} = \tilde{E}\tilde{u},$$

$$\eta \sim \sqrt{\nu\epsilon} \qquad\qquad \epsilon = \kappa/(K_0 r_0^2)$$

The zero-energy mode

$$\tilde{u}_0(\xi) = C(\Delta + k\cosh\xi)^{k\tilde{j}+\frac{\eta\tilde{\Phi}}{2k}}\left(\frac{\Delta+\cosh\xi}{\sinh\xi}\right)^{-\tilde{j}}$$

$$\times\ \exp\left(-\frac{\tilde{\Phi}\Delta\cosh\xi}{2}\right),$$

$$\tilde{v}_0(\xi) = C'(\Delta + k\cosh\xi)^{-k\tilde{j}-\frac{\eta\Phi}{2k}}\left(\frac{\Delta+\cosh\xi}{\sinh\xi}\right)^{\tilde{j}}$$

$$\times\ \exp\left(\frac{\tilde{\Phi}\Delta\cosh\xi}{2}\right),$$

where

$$k = \sqrt{1+\eta}; \qquad \Delta = \Delta(\xi) = \sqrt{1+k^2\sinh^2\xi},$$

$$\tilde{j} = (j + 1/2 - a_\varphi)/\alpha, \qquad \tilde{\Phi} = \Phi/\alpha,$$

Landau states

$$E_n^0 = \pm\sqrt{2n},\, n = 0, 1, 2 \ldots,$$

where the energy is measured in units of $\hbar v_F/l_B$ with the magnetic length $l_B = (\hbar c/eB)^{1/2}$.

$$E_{n=1}^{\eta} \simeq \pm\sqrt{2} \pm \eta\frac{\Gamma}{2\sqrt{2}} \simeq \pm\sqrt{2} \pm 0.3\eta,$$

Landau levels

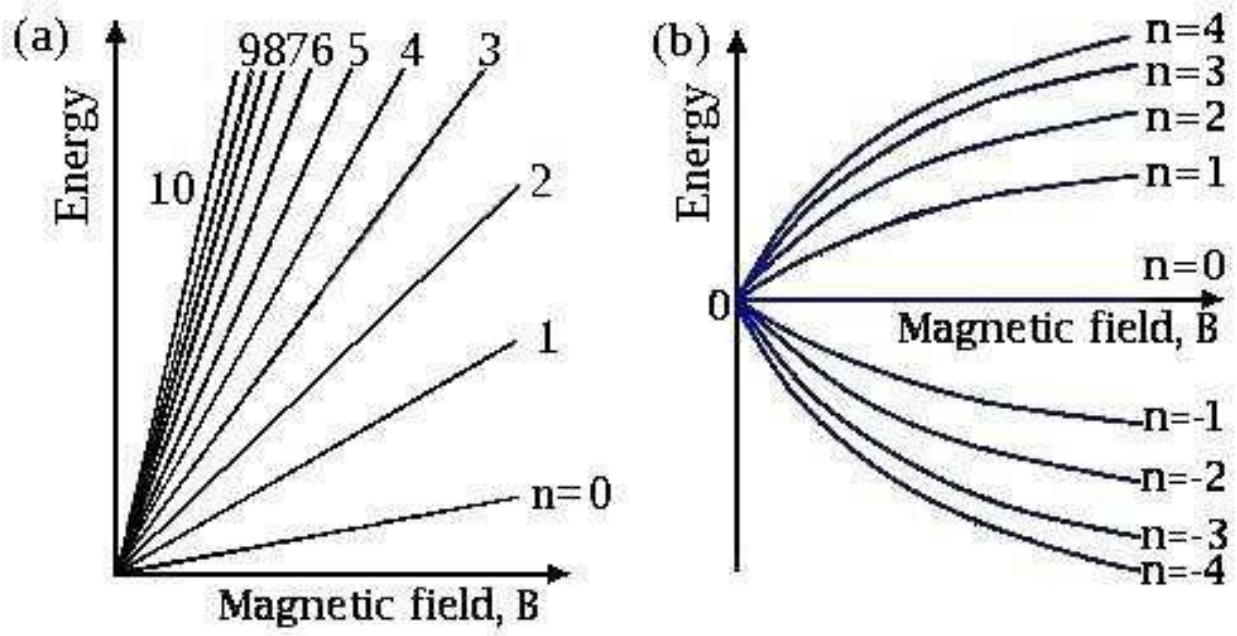

(a) обычные

(b) в графене

Electronic structure
Carbon nanotubes (closed)

metallic

semiconducting

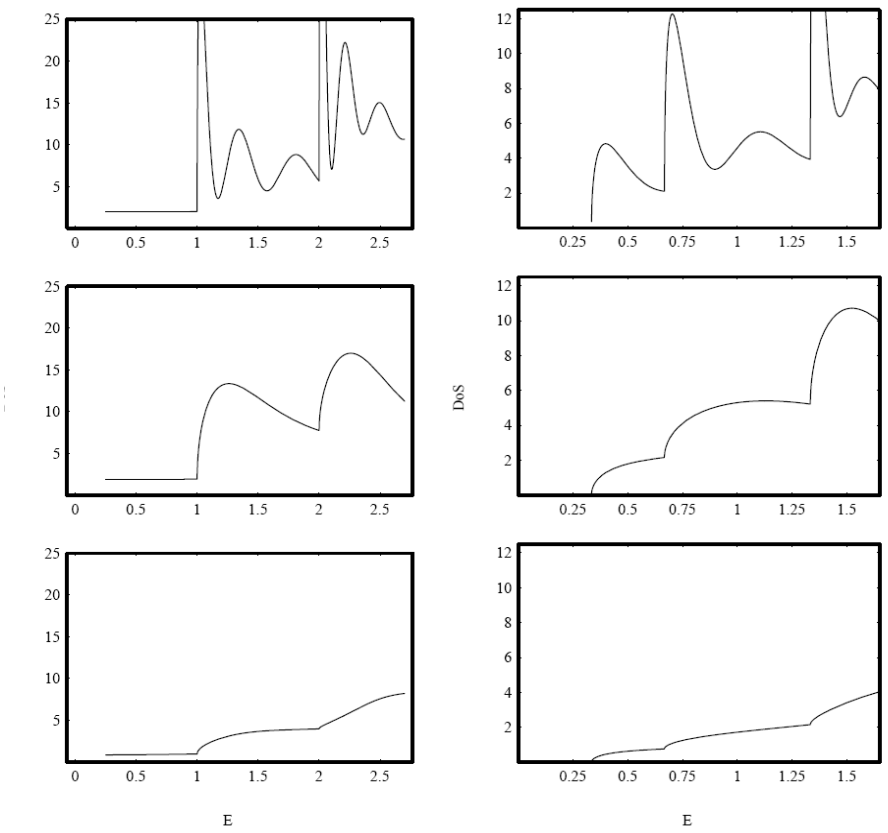

Far from the cap (top), near (middle), in the cap (bottom)

ФИЗИКА ЭЛЕМЕНТАРНЫХ ЧАСТИЦ И АТОМНОГО ЯДРА
2009. Т. 40. ВЫП. 4

ТЕОРЕТИКО-ПОЛЕВОЙ ПОДХОД К ОПИСАНИЮ ЭЛЕКТРОННЫХ СВОЙСТВ УГЛЕРОДНЫХ НАНОСТРУКТУР

Д. В. Колесников *, *В. А. Осипов* **

Объединенный институт ядерных исследований, Дубна

Electronic structure

Spherical and spheroidal fullerenes

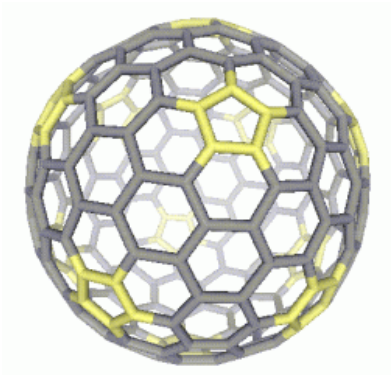

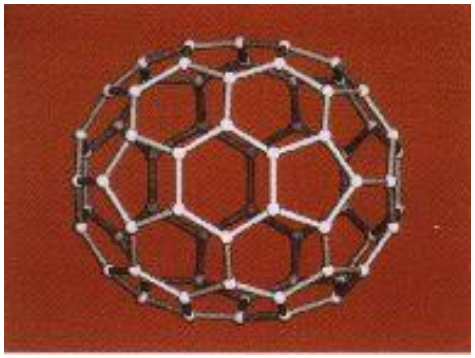

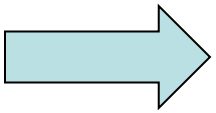

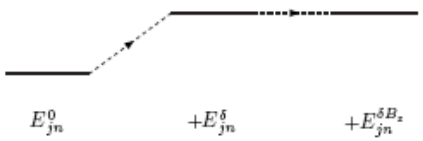

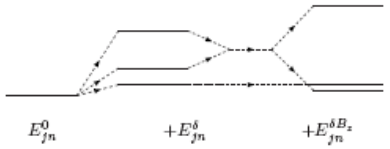

B

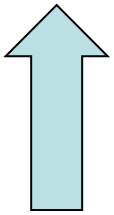

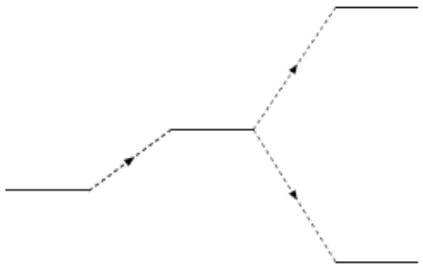

Zeeman splitting

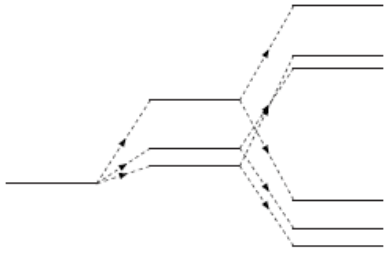

The first electronic level

The second electronic level

Поликристаллический графен

LETTER

doi:10.1038/nature09718

Grains and grain boundaries in single-layer graphene atomic patchwork quilts

Pinshane Y. Huang[1]*, Carlos S. Ruiz-Vargas[1]*, Arend M. van der Zande[2]*, William S. Whitney[2], Mark P. Levendorf[3], Joshua W. Kevek[4], Shivank Garg[3], Jonathan S. Alden[1], Caleb J. Hustedt[5], Ye Zhu[1], Jiwoong Park[3,6], Paul L. McEuen[2,6] & David A. Muller[1,6]

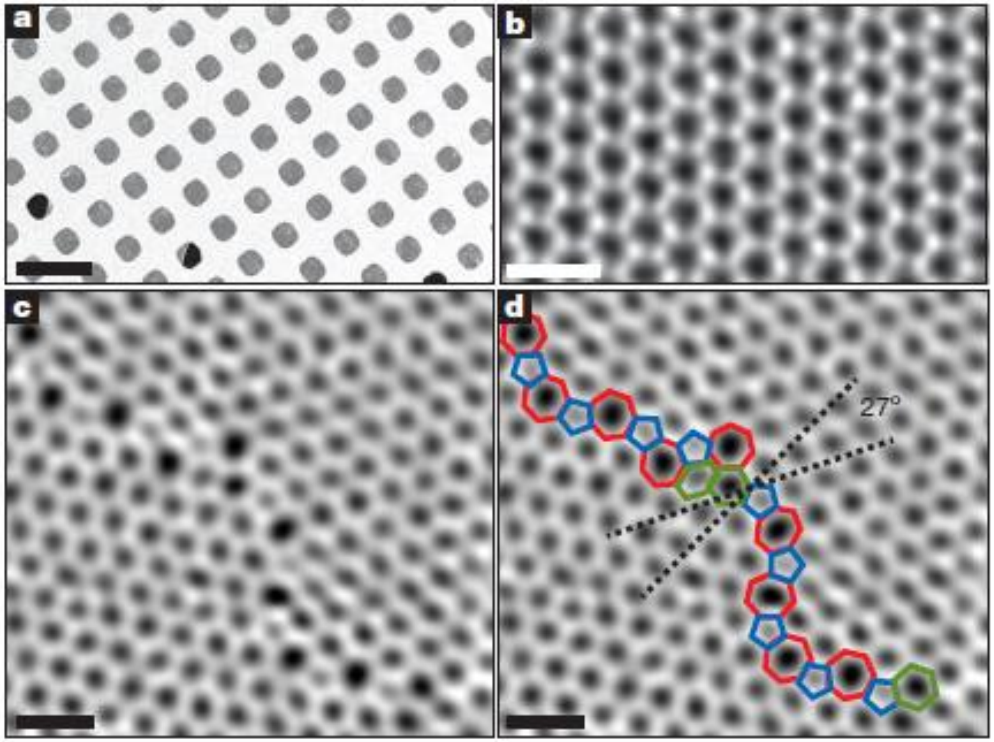

Figure 1 | Atomic-resolution ADF-STEM images of graphene crystals.

SCIENCE VOL 336 1 JUNE 2012

Tailoring Electrical Transport Across Grain Boundaries in Polycrystalline Graphene

Adam W. Tsen,[1] Lola Brown,[2] Mark P. Levendorf,[2] Fereshte Ghahari,[3] Pinshane Y. Huang,[1] Robin W. Havener,[1] Carlos S. Ruiz-Vargas,[1] David A. Muller,[1,4] Philip Kim,[3] Jiwoong Park[2,4]*

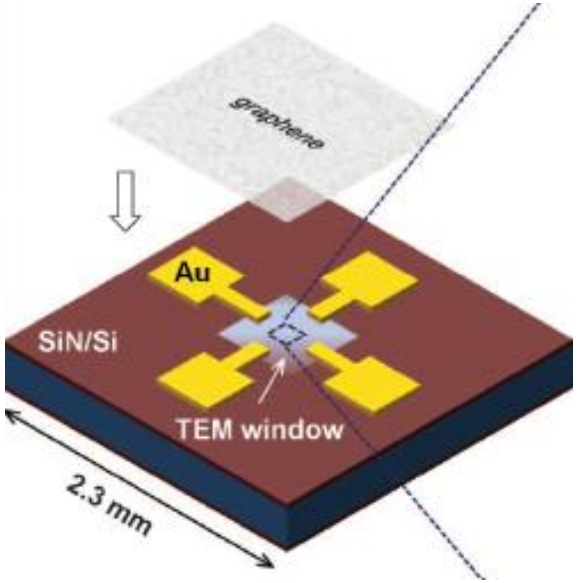

EPL, 100 (2012) 26004
doi: 10.1209/0295-5075/100/26004

www.epljournal.org

Low-temperature thermal conductivity in polycrystalline graphene

D. V. Kolesnikov and V. A. Osipov

Bogoliubov Laboratory of Theoretical Physics, Joint Institute for Nuclear Research
141980 Dubna, Moscow region, Russia

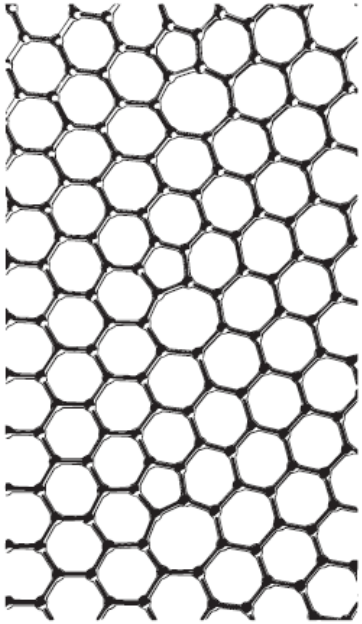

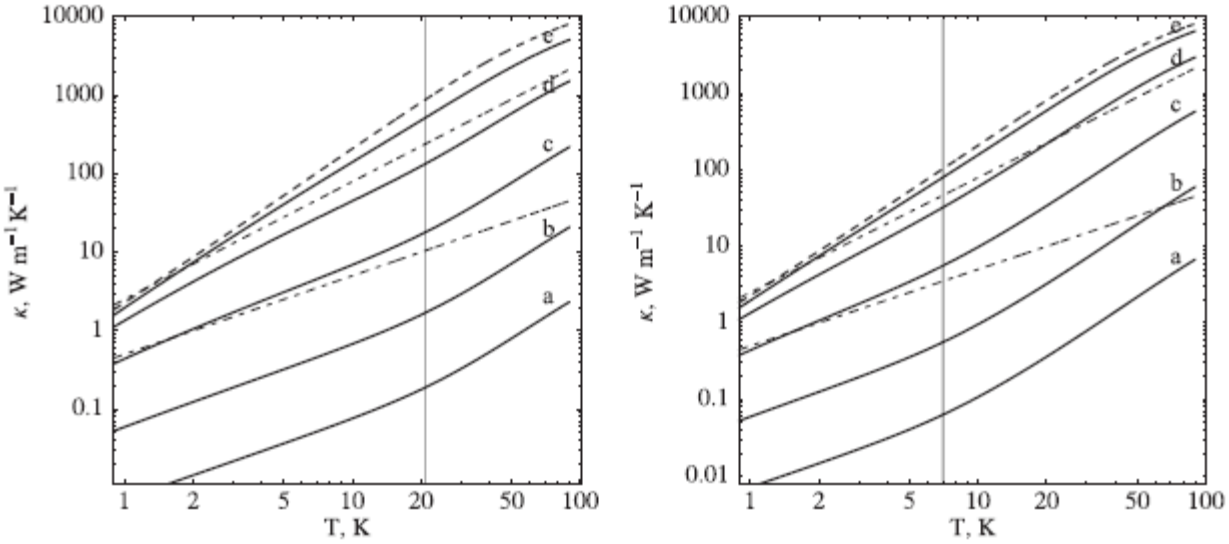

Fig. 2: The total thermal conductivity of polycrystalline graphene with high-angle grain boundaries for $\mathcal{L} = 2.46$ nm (left) and $\mathcal{L} = 7.38$ nm (right) at different packing coefficients: (a) $a/\mathcal{L} = 0$, (b) $a/\mathcal{L} = 2$, (c) $a/\mathcal{L} = 9$, (d) $a/\mathcal{L} = 30$, and (e) $a/\mathcal{L} = 100$ (see table 2). The dashed curve corresponds to the case of the graphene single crystal. The dot-dashed straight lines show $T^{1.5}$ and T. The approximate crossover temperatures are indicated with vertical lines.

Field emission

graphite

carbon nanotubes

few-layer graphene

EFFECT OF BAND STRUCTURE ON FIELD EMISSION

Katkov V.L., Osipov V.A.: J. Phys.: Cond. Matt. 20 (2008) 035204

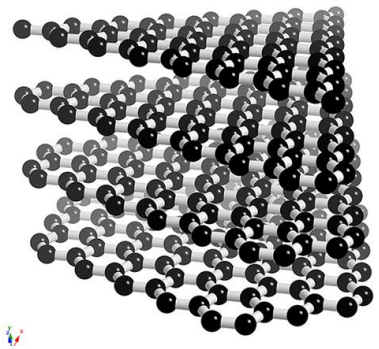

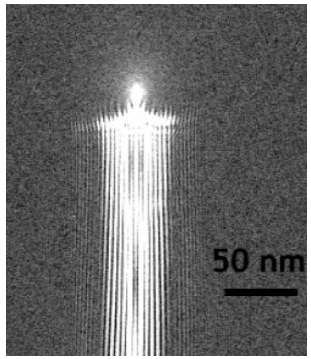

GRAPHITE

NANOTUBES

3D

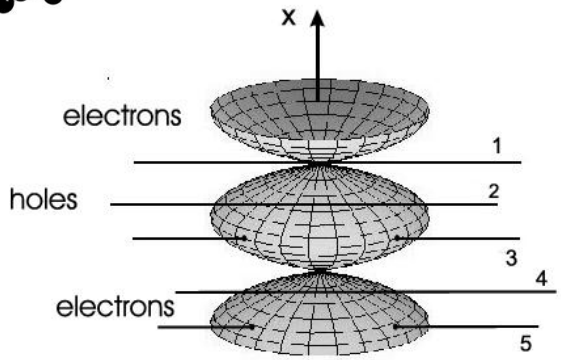

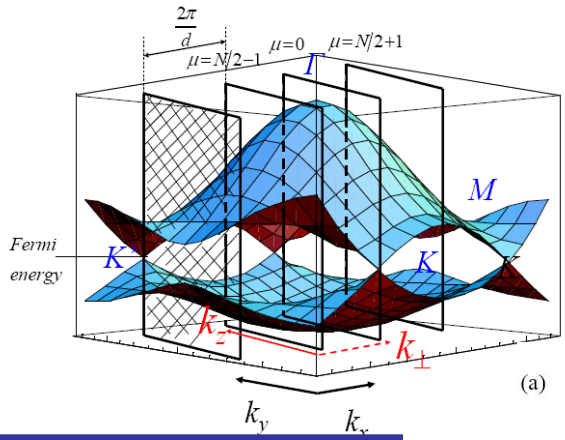

2D

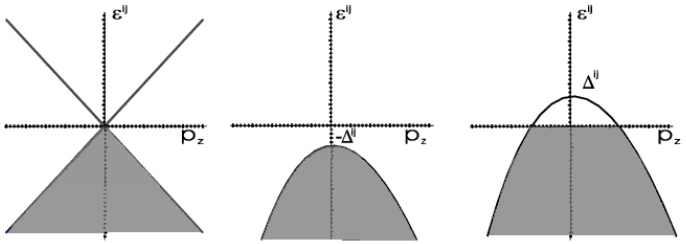

Both cases were reduced to 1D problem.

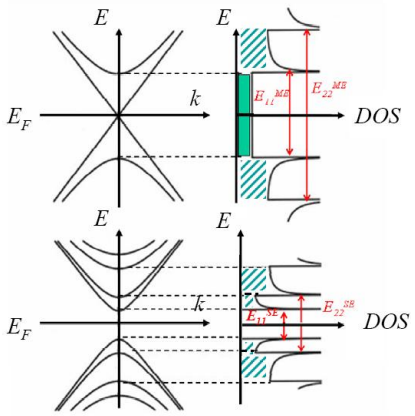

Field emission law for graphite in two orientations.

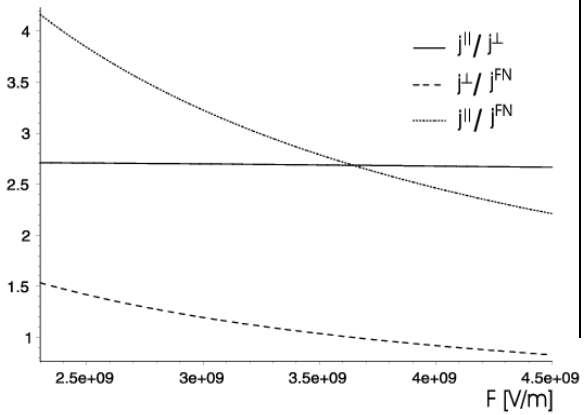

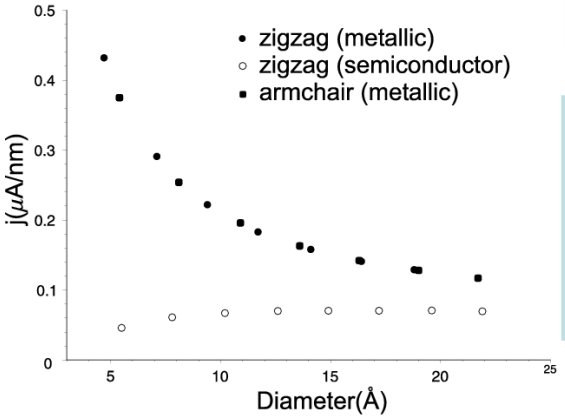

Analytical expressions explain numerical calculations.

Energy distribution of field emitted electrons from carbon nanosheets: manifestation of the quantum size effect

number of layers N

Quantum Size Effect

QSE

quantity of emitted electrons
vs
energy of emitted electrons P(E)
(can be experimentally measured)

FEED

FLG

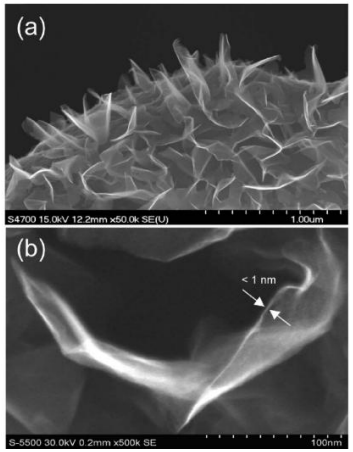

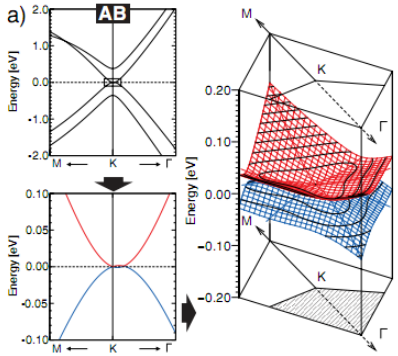

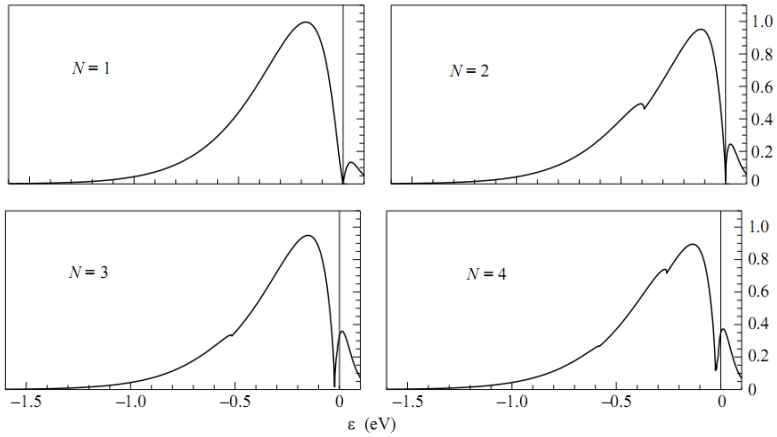

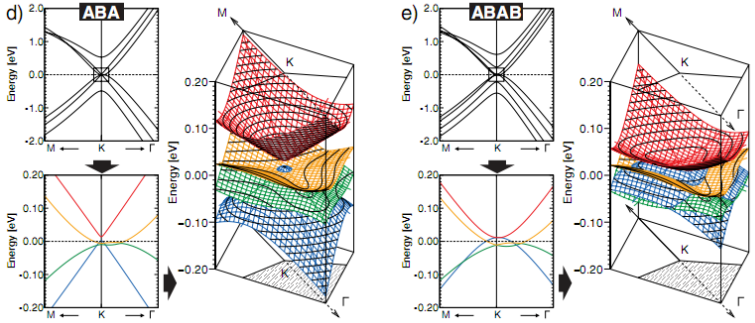

$$P(\varepsilon) = \frac{2g}{v_F} f(\varepsilon) D(\varepsilon) \sum_{n=1}^{n=N} \theta(\epsilon_n) \sqrt{|\varepsilon| \epsilon_n},$$

$$\epsilon_n = |\varepsilon| + \gamma_1^n, \; g = 4e/(h^2 N c)$$

V.L. Katkov and V.A. Osipov, JETP Letters **90,** p. 304 (2009)

Первый шаг к электронному анализу последовательности ДНК: перемещение через нанопоры в графене

(Июль 23, 2010)

(Pennsylvania University, Philadelphia, USA)

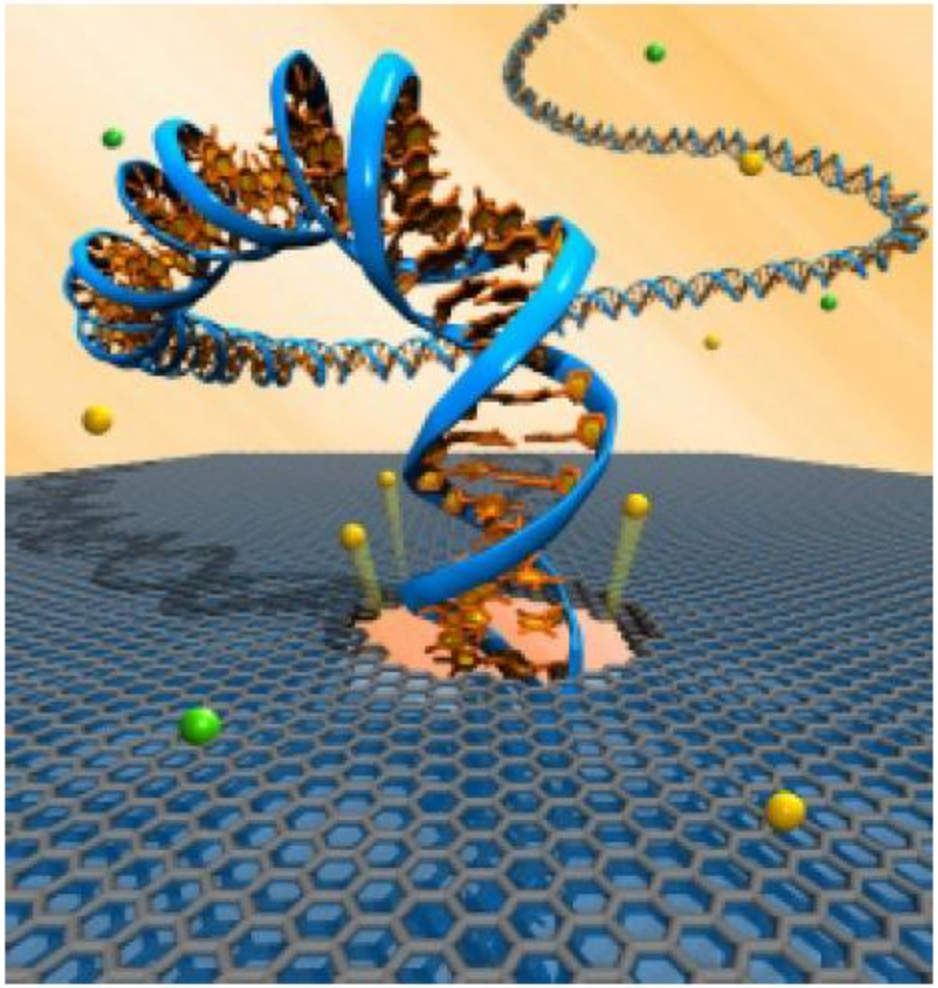

Dubna-Nano 2012 IOP Publishing
Journal of Physics: Conference Series **393** (2012) 012026 doi:10.1088/1742-6596/393/1/012026

Resonant Tunneling In Graphene-DNA Base-Graphene Junctions

V.L. Katkov, O.G. Isaeva and V.A. Osipov
Bogoliubov Laboratory of Theoretical Physics, Joint Institute for Nuclear Research, Dubna, Russia

Наши расчеты

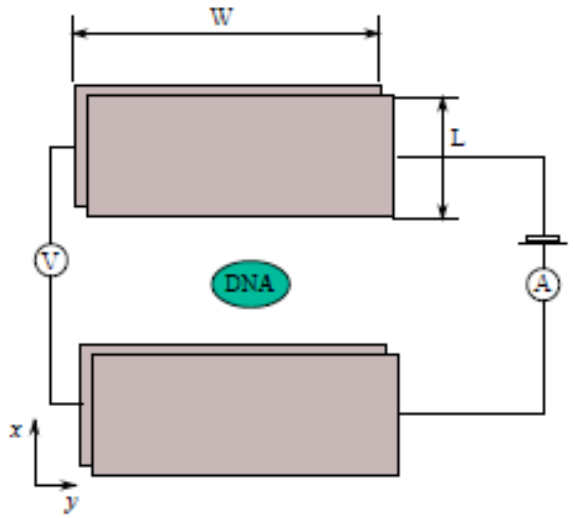

Схематическое изображение устройства

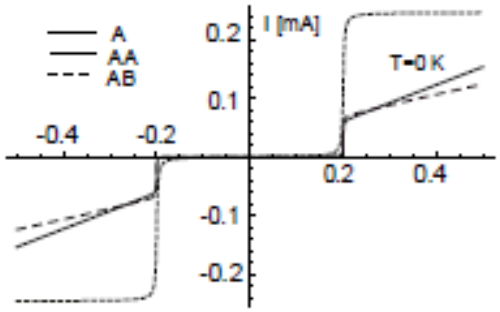

Рис. 2. $I - V$ характеристика туннельного контакта при нулевой температуре

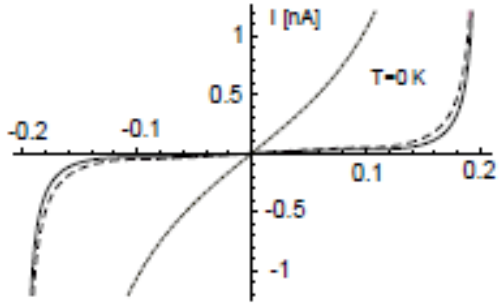

Рис. 3. Центральная часть вольт-амперной характеристики

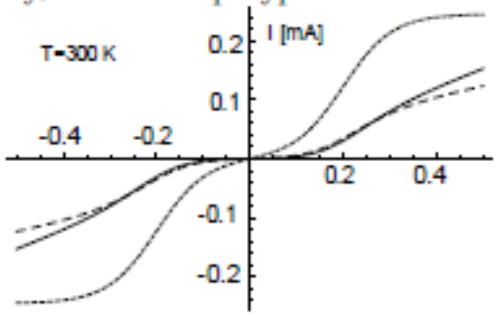

Рис. 4. $I - V$ характеристика туннельного контакта при комнатной температуре.

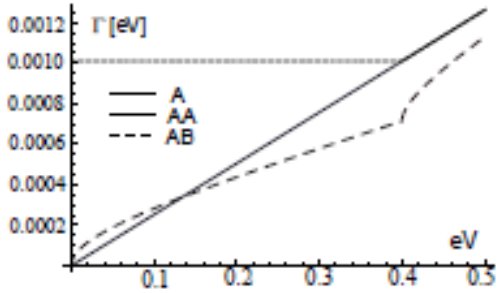

Рис. 5. Зависимость темпа туннелирования от эрергии, отсчитанной от уровня Ферми